Pressure variations in the northern part of the Danish Central Graben, the North Sea.

By: Ole V. Vejbæk, Hess Denmark Aps, - now at AkerBP ASA.

The overpressure variation in the Cenozoic to Jurassic succession in the northern part of the Danish Central Graben may broadly be divided into three major compartments: An upper hydrostatically pressured unit comprises the post-mid Miocene to recent succession down to $\sim 1200m$ depth in the North and $\sim 700m$ in the South part of the Danish Central Graben. The second compartment comprises the mid-Miocene smectite rich clays down to and including the upper Cretaceous chalk. There, the Paleogene to Lower Miocene succession provides the seal. The third compartment constitutes the Jurassic succession with pressure above hydrostatic that may exceed twice that seen at the upper chalk level. Pressure levels can be estimated using Eaton's approach for the second compartment in agreement with pressure data. Modeling of the transient pressure development in the Cretaceous — mid-Miocene succession broadly complies with Eaton estimates and show main overpressure build-up to occur within the last $10Ma$. The overpressure in this succession may be mapped using methods that exploit correlations between fluid pressure and degree of consolidation,- while the Jurassic cannot. However, the lateral variation of the upper Jurassic overpressure correlates broadly with the maturity of the Upper Jurassic source rock allowing the pressure variation to be mapped.

The spatial and temporal variation in pressure in the Danish Central Graben is analyzed with main focus on the northern part of the area (Fig. 1). Broad pressure variation in this area has been studied previously by Japsen (1999) and Dennis et al. (2005) with emphasis on the Cretaceous - Paleocene chalk which contains the main hydrocarbon reservoirs in Denmark. However, these studies have only minor focus on a key objective in this study, the vertical pressure variation as required for well stability analysis related to drilling. It is common practice in the industry for the purpose of drilling to estimate pressure variation above the chalk using indirect indicators of pressure such as seismic velocity variation,- but rarely supported by other means of deriving pressure such as forward modeling of the pressure development.

Pressure estimates are here obtained by Eaton analysis corroborated by basic forward modeling of pressure presented below and in the appendix and compared with direct observations (Table 1). The applied forward modeling only assumes overpressure to be generated by sediment loading as may be implicit in the Eaton analysis. The forward modeling may therefore support Eaton estimation to help avoid some of the inherent associated pitfalls and may in addition provide timing of overpressure generation.

Onset of overpressure, when portrayed in a pressure - depth plot, defined as pressure above hydrostatic, is observed in many wells to occur in the mid-Tertiary and build downwards towards the Cretaceous - Paleocene chalk. Overpressure is within the range 5 to $20MPa$ at the upper chalk level at 2 to 3km depth. In the Jurassic overpressure is observed to be anywhere from similar to chalk overpressure to exceed $40MPa$ (compared to hydrostatic pressure of $\sim 46MPa$ and a total pressure of $86MPa$ at 5 km).

The general lithostratigraphy in the area is provided by Schiøler et al. (2007), overview of spatial lithological variation in the area can be obtained from Rasmussen (2005) and Rasmussen et al. (2013), and a local example may be provided by the Amalie-1 well (Fig. 2). This well also provides an excellent overview of the pressure variation. Overpressure starts in the mid-Tertiary at around $1200m$ increasing downward. No pressure measurements are available in this well to support the estimate in the Cretaceous to Tertiary succession, but is based on modeling supported by observations in adjacent wells. However, the well has several pressure measurements in the Jurassic to show a water gradient shifted up by an overpressure above hydrostatic in the order of $43.4MPa$. This extends from the top Jurassic to a depth of $\sim 5km$, where a further increase is seen to around $52MPa$,- probably coinciding with the top of the gas window (Damtoft et al. 1992; Petersen et al. 2016; Pletsch et al. 2010). It is important to distinguish between local gradients and average gradients as would be calculated from mud-weights; the latter is only practical in connection with the drilling process.

Whether or not the pressure increase into the Jurassic takes place across the lower Cretaceous or just across the tight lower part of the chalk is not known in

detail. No pressure measurements are available there in this well, and as is discussed below, indicators of consolidation like sonic data cannot resolve this. However, sparse pressure data from other wells in the study area suggest that both the lower tight chalk and the Lower Cretaceous may seal the high pressure in the Jurassic.

The succession in the Amalie-1 well is divided into 3 main pressure units: a post-mid-Miocene hydrostatic pressure succession, moderate overpressure in the Upper Cretaceous to mid-Miocene succession and a Jurassic succession with extreme overpressure. Extreme overpressure is here defined, not by absolute values but as pressure coming close to the fracture gradient. The further pressure increase observed in Amalie-1 at around $5km$ is only documented in a couple of wells in the area. It is noted that pressure appears to drop from the top of the Jurassic and downwards in the mudweight plot from the final well report (Fig. 2 left), which is an artifact of normalizing to specific gravity (averaged to depth); in reality the overpressure (pressure above hydrostatic) is constant in the Jurassic down to $\sim 5km$.

Overpressure in the general North Sea Central Graben area has been the subject of many studies (e.g. Hunt 1990, Powley 1990, Ward et al 1994, Osborne and Swarbrick 1997, Dennis et al. 2005). Powley (1990) recognized a similar three-fold subdivision for the southern Norwegian North Sea adjacent to the study area of this paper. Powley (1990) observed that pressure seals are not layer-specific but seem to follow specific depths. Japsen (1999) demonstrated a broad correlation between the interval velocities and overpressure of Lower Cenozoic shales in the greater North Sea area. He attributed the cause of the pressure to rapid Neogene deposition causing disequilibrium compaction. In this paper, the disequilibrium compaction mechanism is analyzed further. Both Japsen (1999) and Dennis et al. (2005) show maps of regional variation of overpressure at the top Chalk level.

Ward et al. (1994) recognized the existence of two domains of overpressure in the Central Graben area; a Mesozoic system (Jurassic mainly) of extreme overpressure generated by unloading and sealed by the deeper chalk,- and a Tertiary -Upper Chalk system of moderate overpressure caused by disequilibrium compaction. They proposed the unloading mechanism of the Jurassic system to be due to fluid expansion related to hydrocarbon generation. Ward et al. (1994) proposed a fairly discrete "fluid isolation depth" to provide top-seal for the lower Tertiary-Cretaceous system, and suggested low porosity chalk ($< 5\%$), not following any specific horizon, to provide the seal between the upper chalk moderate and the higher pressure Jurassic.

Osborne and Swarbrick (1997) provide an overview of mechanisms that may generate overpressure. Of the 11 different mechanisms discussed by them, the most realistic options for the study area appear to be disequilibrium compaction, and kerogen transformation, in particular gas generation.

Mapping of overpressure most commonly exploits a relationship between porosity or proxies like velocity or resistivity and effective stress as in the Eaton analysis. This assumption is investigated for the second compartment (mid-Miocene to upper Cretaceous chalk). Nordgård Bolås et al. (2004) discussed that dis-equilibrium

compaction plays only a minor role for overpressured Jurassic shales in the Norwegian North Sea, as they observed porosity levels similar to those for hydrostatic pressured shales and yet extreme pressure. Hence unloading pressure build-up must be of major importance. The Jurassic in the study area of this paper have similar low to moderate porosity despite extreme pressure.

Background

It is recommended to always bear in mind that overpressure may build and dissipate on geological timescales as described by the basic transient pressure equation:

$$\frac{\partial P}{\partial t} = \kappa \nabla^2 P \tag{1}$$

$$\text{where} \nabla^2 P = \frac{\partial^2 P}{\partial x^2} + \frac{\partial^2 P}{\partial y^2} + \frac{\partial^2 P}{\partial z^2}$$

as is also the premise in this paper. Left side is the temporal pressure dissipation rate. The main factors on the right side are the second spatial derivative to pressure, the Laplacian of the pressure, which represents the anomaly,- and the pressure diffusivity:

$$\kappa = \frac{K}{\phi c_e \mu} \tag{2}$$

which determines the dissipation rate of the anomaly.

Assuming variations in the porosity (ϕ), and viscosity (μ) to be minor, it is clear that permeability (K) and effective compressibility (c_e) are of primary and equal importance for determining the pressure dissipation rate as these can vary by orders of magnitude. Unless both permeability is sufficiently low and compressibility is high to make κ sufficiently small, overpressure is likely to dissipate too fast to remain significant in geological time. If κ is too large, the second derivative of pressure (in space) quickly goes to zero with time, which means that the first derivative is a constant: zero laterally and defined by fluid density vertically: $\frac{\partial P}{\partial z} = g \cdot \rho_w$. The local vertical pressure gradient therefore cannot differ much from the hydrostatic gradient,- even within pressure compartments, unless κ is at similarly low levels as required in sealing successions.

Thus, local pressure gradients will be lower than typical mud weight gradients in permeable sections, even if these are overpressured. Perhaps less obvious is that high-frequency overpressure results in large values of the second derivative locally that therefore will dissipate fast. This makes high-frequency variation in overpressure unlikely, and as a rule spatial pressure variation will be smooth.

The system compressibility is found from the sum of grain, fluid and bulk compressibility. Since the pressure anomaly in the chalk overburden is of the disequilibrium compaction type (cf. Vejbæk 2008), the bulk compressibility is the

plastic compressibility describing compaction (uniaxial plastic deformation or pore-collapse). As discussed below, plastic compressibility is likely several orders of magnitude larger than water and mineral phase compressibilites as well as bulk rock elastic compressibility. Hence plastic compressibility will dominate the pressure diffusivity unless unloading has occurred. Hydrocarbons, especially gas, may also have large compressibilities to reduce pressure diffusivity.

Muggeridge et al. (2005) discuss the significance of fluid compressibility rather than bulk compressibility for abnormal pressure to last for geological time-scales. They assume elastic bulk compressibility, which would be the case for unloading overpressure. However, the presence of hydrocarbons may increase compressibility significantly to allow overpressure due to un-loading to last in geological time-scales as required for the Jurassic overpressure.

Equation 1 is solved numerically to estimate the temporal pressure development under the assumption that vertical pressure dissipation is dominating. Thus, equation 1 reduces to:

$$\frac{\partial P}{\partial t} = \frac{K}{\phi c_e \mu} \frac{\partial^2 P}{\partial z^2} \tag{3}$$

For clarity and to allow comparison of overpressures observed at different depths, the total fluid pressure (P_{fluid}) is subdivided into hydrostatic pressure (P_h) and overpressure (pressure above hydrostatic; P_e):

$$P_{fluid} = P_h + P_e \tag{4}$$

In this paper, results are mainly presented as pressure above hydrostatic (P_e values). Hydrostatic pressure is given by:

$$P_h = g \int_0^z \rho_w \partial z \tag{5}$$

where g is acceleration due to gravity, and ρ_w is brine density. If the brine density can be assumed constant, the equation simplifies to: $P_h = g \cdot z \cdot \overline{\rho}_w$, where $\overline{\rho}_w = 1050 Kg/m^3$ is the assumed average density.

The vertical stress (σ_v) is similarly found by integrating the bulk density (ρ_B) of the sediments. If the density log is incomplete, an average sediment density of $2000 kg/m^3$ is typically used to fill minor gaps in the log data.

Compaction is assumed driven by increases in effective (vertical) stress as defined by the Terzaghi equation:

$$\sigma'_v = \sigma_v - P_{fluid} \tag{6}$$

where the apostrophe signifies effective stress.

Compaction is assumed to reduce porosity (ϕ) according to:

$$\phi = \phi_0 \cdot e^{-a \cdot \sigma'_v} \tag{7}$$

where ϕ_0 is porosity at the time of deposition (sediment surface). This equation is similar to the compaction decay model proposed by Athy (1930), except by replacing the depth (z) by effective stress (σ'_v). This allows reduced compaction due to over-pressuring to be accounted for. An important caveat, however, is that effective stress must be ever-increasing albeit slowed down when overpressure builds. This is inherent in the assumption that compaction is plastic, hence irreversible. This assumption is also implicit in most indirect methods for assessing overpressure based on degree of consolidation as for instance the Eaton method (Eaton 1975). When pressure builds such that effective stress reduces (un-loading), then the relationship in equation 7 is no longer valid. Indirect ways of estimating pressure like the Eaton method, will therefore fail in such situations because there is no longer a simple relationships between degree of consolidation and pressure. In addition the diffusivity will increase because plastic compressibility no longer applies.

Direct pressure observations

In this paper, primary data are down-hole pressure measurements obtained with tools that isolate well bore sections and measure pressure locally. These include the Repeat Formation Tester tool (RFT), the similar Modular Dynamics Tester tool (MDT) and Drill Stem Tests (DST) (Table 1). Eighteen wells with such pressure points have been used in the study and are supplemented with a couple of wells having only indirect pressure data as discussed below (Table 1). Typically several RTF and MDT pressure points are measured at the zone of interest but in Table 1 only one representative depth is listed. The absolute measured pressure corresponding to each point is found by adding the hydrostatic pressure given by the depth ($P_h = z \cdot g \cdot \rho_w \cdot 10^{-6} MPa$, where $\rho_w = 1050 Kg/m^3$) to the overpressure (P_e) in Figs 16 and 18). The variation in the chalk pressure data is attributed mainly to variations in burial history; primarily variations in thickness of the sealing succession and Neogene deposition rates (Fig. 3).

Mud-weights applied during drilling of the wells are of lesser value and are not considered hard data. Useful information may only be where fluid gains have been observed, if the depth of the gain is known. Mud-weights are typically selected for stable drilling and are at or above formation pressure. The mud pressure gradient is broadly the same in the well bore from the surface to the depth where overpressure is encountered (deviations are mainly due to circulation dynamics). The well pressure will typically be higher than the formation pressure in the shallower hydrostatic pressured section. For the same reasons, the mud pressure will often be higher than formation pressure deeper than the depth where high-pressure inflows were encountered, especially if the overpressured parts of the succession are internally permeable (small pressure diffusivity; equation 2).

Indirect pressure estimates

A common way to estimate overpressure in the absence of measurements is to assume (often implicitly) correspondence between the degree of compaction and present-day effective stress such that proxies for the degree of compaction may be translated directly to effective stress. A well-established method of this type, is the one initially proposed by Eaton (1975) using sonic log data:

$$P(obs) = \sigma_v - (\sigma_v - P(N)) \left[\frac{V_p(obs)}{V_p(N)} \right]^n \tag{8}$$

where σ'_v is vertical effective stress and V_p is p-wave velocity and N and obs refer to the hydrostatic and observed trends respectively. The method thus requires a normal trend to be defined to which a least squares fit is done to determine the exponent n. An exponent of 2 was used in all wells with useable velocity data.

A convenient form for the normal trend is:

$$V_p(N) = b \cdot \exp(a \cdot \sigma'_v(z)) \tag{9}$$

where parameters a, and b are fitted to hydrostatic pressured sections of the sonic log data. The vertical effective stress is found by integrating the bulk density log data to yield vertical effective stress at all depths, and subtracting the pressure, which is straight forward when pressure is hydrostatic (equation 6).

In the study area, the velocity function defining the normal compaction trend (hydrostatic conditions) was estimated by a least squares fit of sonic data to equation 9 selected for $Z < 1240m$ including only clay-rich intervals ($V_{cl} > 0.66$). Clay-rich intervals deeper than this showed to deviate clearly from the fit, which is assumed to indicate deviation from hydrostatic conditions.

The validity of the definition of the hydrostatic pressured section is based on obtaining a good fit for the hydrostatic pressure gradient consistent with equation 5, obtaining a clear definition of onset of overpressure, and ideally supported by direct measurements if available. In the study area, several wells have direct measurements as discussed below but only from the chalk or thin sands resting on or just below the chalk. Pressure cannot be measured in the Tertiary shale using standard techniques.

After converting sonic velocities to m/sec, constants were found to be $b = 1850$ and $a = 0.0227$ in general for the entire chalk overburden in the studied wells but with minor variations from one well to another. Similar studies of velocity – depth functions (here depth is replaced by effective stress), commonly yield a values that are negative in line with an assumed asymptotic approach to a finite high velocity at high stress and/or zero porosity (e.g. Hermanrud and Undertun 2019). However, the available data in the study area suggest a slightly accelerating trend with depth, which limits the validity range for the fit. The fit applies to the normally pressured section (above $\sim 1200m$) but is required to be valid down to the chalk level. It is conjectured that the positive a value reflects a near surface velocity increase that may be due to glacial effects as discussed below.

An example fit is shown in Fig. 4 using velocity data from the Rigs-4 well, where clay rich intervals used for the fit are shown with green crosses. There, the general velocity level was a bit lower and the b value reduced to $1800m/sec$ with a standard deviation of $27m/sec$. Also in this well, the normal function fit complies with the positive a value in equation 9.

Similarly, resistivity log data can be deployed:

$$P(obs) = \sigma_v - (\sigma_v - P(N)) \left[\frac{R(obs)}{R(N)} \right]^n \tag{10}$$

where $R(obs)$ is logged resistivity in Ωm, and $R(N)$ is the trend resistivity corresponding to normal pressure. The optimal n exponent for resisitivity data was found to be 0.45.

Importantly, it is implicitly required that minor lithological variation can be ignored for both sonic and resistivity data, and that the fit defines the average behavior in the interval where it is applied. In this context, it may be a problem that the normal trend must be estimated in the hydrostatic pressure section and assumed valid for the overpressured section if pressure is estimated using the Eaton analysis. The inability to obtain pressure measurements in the clay to which the Eaton parameters are fitted also hampers direct quality control on the estimate, and must rely on assumed continuation of pressure levels into adjacent sand or chalk formations where pressure can be obtained. Apparent minor fluctuations in pressure may reflect minor variation in lithology as real high frequency pressure variation will dissipate faster than low frequency variations,- and major changes in lithology may erroneously be interpreted as major changes in overpressure.

Another important implicit assumption is that higher effective stress has not occurred in the geological past, as consolidation can be assumed to be broadly irreversible. The effects of unloading on this kind of indirect pressure estimation are discussed by Bowers (1995) with a focus on sonic data. He estimates velocity reductions resulting from unloading to be much less (almost an order of magnitude) than the corresponding velocity increase during consolidation (loading). Hence complications originating from for instance variations in lithology can easily dwarf subtle velocity reductions from unloading. The use of resistivity for Eaton analysis includes further complication due to salinity variations and temperature effects on resistivity. Increased salinity may cause an apparent increase in porosity, and increasing temperature may reduce resistivity.

Application of Eaton analysis

Examples from the Danish Central Graben area of applying the Eaton type analysis include the Rigs-4 well using velocity data (Fig. 5a) and the Bertel-1 well using resistivity data (Fig. 5b). The light green curves are the Eaton estimates, and in red are model estimates (forward pressure modeling discussed below). In the Bertel-1

well, a normal compaction trend (ie. at hydrostatic pressure) is indicated shallower than $\sim$ 1250m, and below a gradual downward increase in overpressure is seen reaching just over 14MPa at chalk level as confirmed by pressure measurements in wells near to Bertel-1. In the Rigs-4 well, a DST from inside the chalk is consistent with the downward extrapolated fit from above the chalk. Both wells appear to return to hydrostatic pressure, or even below, in the chalk. This is an artifact of a lithological change from clay-rich sediments to chalk to which the defined Eaton compaction trend does not apply. The complex compaction behavior of chalk is discussed by for example Fabricius (2007) and Fabricius and Borre (2007), and is not analyzed for pressure estimation in this paper.

The apparent high-frequency variation in the Eaton estimate is attributed to more subtle lithological variation. Apparently, the Rigs-4 well has pressure exceeding the model estimate just above the chalk. In addition to high granularity fluctuations, this too is interpreted to be an artifact of lithology. Clay types may vary considerably in the Paleogene of the North Sea (e.g. Nielsen et al. 2015); particularly kaolinite may lower sonic velocity considerably to erroneously indicate further increased pressure (cf. Mavko et al. 1998).

In Fig. 6 *a* and *b*, Eaton analysis for the Diamant-1 well is shown using both sonic and resistivity data. Both methods appear to produce pressure estimates in the Tertiary at comparable levels. Again the Eaton estimate defined in the overburden clearly does not apply to the chalk, and show significant difference depending on input data type. Below the chalk, results based on sonic and resistivity data differ but neither reach the levels measured at the base of the well in the Jurassic. Similar to Bertel-1, the Diamant-1 well appears to return to an overpressure level in the Jurassic that compares to above the chalk judging from the Eaton derived pressure estimates if the calibration was valid for the Jurassic as well. This may not be the case.

The Upper Jurassic Farsund Formation lithology is clay-rich siliciclastic sediments, broadly comparable to the Tertiary clays. Thus, the analyses appears to indicate pressures at similar levels rather than being a lithological artifact. However, pressure measurements show pressure to be at $\sim$ 35MPa above hydrostatic at the Bertel-1 location and $\sim$ 26MPa at the Diamant-1 location; at least twice the overpressure seen at top chalk level.

The failure of the Eaton analysis to capture Jurassic pressure, at least with the post chalk calibration, is attributed to a mechanism of unloading by hydrocarbon generation in the rich source rocks of the Farsund Formation (e.g. Petersen et al. 2010) rather than dis-equilibrium compaction. Nordgård Bolås et al. (2008) have similarly observed too low porosity considering the observed pressure (too low effective stress) in Jurassic strata in the Norwegian North Sea. They attribute stress insensitive diagenetic processes to be the cause not only for the lower porosity but also the unloading overpressure rather than hydrocarbon generation. They are inclined to assume hydrocarbon generation to be a too feeble mechanism unless gas is generated.

The Eaton analysis appears to pin-point the depth where pressures start to exceed hydrostatic in the Tertiary based on where the estimated pressure curve starts deviating from the hydrostatic curve. Due to impermeable nature of the sediments, validation by direct pressure measurements is not possible. In the profile in Fig. 7, this level is approximately at the thin dark red line,- clearly cross-cutting seismic reflectors. As already pointed out by Powley (1990), it is not at a specific stratigraphic level (or seismic reflector) that defines the top overpressure. It rather seems to correspond to the toe-set portion of the mid to upper Miocene low-angle prograding succession seen in Fig. 7 (Rasmussen 2013, Schiøler et al. 2007).

The succession riddled by numerous intraformational normal faults between top chalk and top overpressure is seen to start some distance below the top of the overpressure at near Top Lark Formation level (Fig. 7). The top of the disturbed zone has traditionally been assumed to define the top of the overpressure by seismic interpreters. That this may not be the case, is consistent with the Mohr- Coulomb theory for normal faulting, as the top of the overpressure also represents a local maximum in effective stress (see below) and thus the least likely place for normal faulting to occur in the over-burden (Vejbæk 2008). However, if the downward increase in pressure above hydrostatic would be much lower than suggested by the data here, this effective stress maximum could vanish.

Compaction

Consolidation is assumed to take place through uniaxial compaction assuming no lateral strain in response to effective stress increases. The compaction is guided by the bulk plastic compressibility (e.g. Dake 1978), which is approximated by the derivative of the porosity - effective stress relationship:

$$c = \frac{\Delta V}{V}\frac{1}{\Delta p} = \frac{\Delta H}{H}\frac{1}{\Delta p} \sim \frac{\partial \phi}{\partial \sigma'} \tag{11}$$

The Eaton analysis includes defining a normal consolidation trend for velocity and resistivity. The interval velocity for Tertiary clays as a function of effective stress in equation 9 is shown in Fig. 8. The generalized hydrostatic velocity - depth trend is indicated by an approximate depth scale (in case of hydrostatic conditions). The previously discussed increasing velocity - stress gradient with depth is not typical for such relationships and originates from the least squares fit and should not be used for extrapolation to higher stresses. Application of an empirical Gardner type relationships between V_p and ρ_B results in the density - effective stress trend seen in Fig. 8 second plot (cf. Mavko et al. 1998). Further transformation of density to porosity (brine density of $\rho_w = 1030 Kg/m^3$ and mineral density of $\rho_S = 2660 Kg/m^3$) produces the third plot in Fig. 8; the porosity - effective stress (depth) trend. A fit to the exponential porosity - effective stress curve given in equation 7 yields the parameter values: $\phi_0 = 0.46$ and $a = -0.0671$ (assuming σ'_v in MPa) as shown in red in Fig. 8. These parameter sets represent the average

(implicit assumption in Eaton analysis) for the Tertiary sealing succession but is only used below for assessment of the average pressure diffusivity deployed in forward modeling.

From the derivative of this function, the compressibility is found to be in the range: $c_b = 2.5 \cdot 10^{-8} Pa^{-1}$ (surface) to $c_b = 0.5 \cdot 10^{-8} Pa^{-1}$ at $\sigma'_v \sim 40 MPa$ (fourth plot in Fig. 8). In comparison, brine compressibility is in the order of $4 \cdot 10^{-10} Pa^{-1}$ considering realistic depth, temperature and salinity ranges (e.g. Mavko et al. 1998). This range in plastic compressibility is similar to estimates found by Nordgård Bolås et al. (2004) in the Norwegian North Sea. Their porosity - depth trends for a selection of clay-rich formations show only moderate variation suggesting an equal moderate variation in plastic compressibility. Results from forward modeling of the compaction in the study area in this paper, suggests that the maximum effective stress reached is less than $15 MPa$ in the overburden (see below).

Permeability is difficult to estimate in the lab and in the field. Mondol et al. (2008) provide general laboratory-based effective stress - permeability relationships for various clay minerals where smectite rich clay have the tightest trend and kaolinite a more permeable trend. Mondol et al. (2008) investigate the effect of consolidation on permeability from effective stresses of zero to $50 MPa$. At zero stress, the porosity starts at 70% in their experiments, while the average porosity trend found here indicates $\sim 47\%$ porosity at surface (Fig. 8). The discrepancy in surface porosity may be due to glacial loading affecting the area during the Pleistocene that also may be reflected in the average velocity - effective stress function discussed above (e.g. Medvedev et al. 2020).

The Pleistocene glacial - interglacial cycles have a duration of around 100,000 years of which roughly 20,000 years define the periods of maximum extent of the ice-sheets to cover most of the North Sea (e.g. Bendixen et al. 2018, Huuse and Lykke-Andersen 2000). More recent estimates of ice-thicknesses suggest $500m$ as typical in the North Sea (e.g. Medvedev et al. 2020). The ice-sheet would clearly not cause neither over-pressuring nor compaction if the ice was floating in sea-water as seen from the Terzaghi equation (equation 6). However, the global sea-level drop associated with the glaciations far exceeds the current water-depth in most of the North Sea as corroborated by observations of channels formed under ice and glaciotectonic deformations of the near surface sediments (e.g. Huuse and Lykke-Andersen 2000, Kristensen and Huuse 2012). Therefore, the elevated fluid pressure may have started to dissipate while the increased lithostatic stress was still high.

The ice-loading effect may be illustrated by the modeling shown in Fig. 9, where an ice-load of $500m$ thickess is applied for 20,000 years resulting in a temporary load of $4.5 MPa$. Both vertical stress and pressure are increased by the same amount initially with no immediate change in effective stress. This loading rate is orders of magnitude faster than the sediment loading rate and due to the short duration of the load pressure dissipation is negligible except for the most permeable and compressible near surface layers. Thus, pressure dissipation only occurs in the the upper few hundred meters despite an increased pressure diffusivity by of factor

of 50 compared to the one used for the deeper over-pressured section in this experiment. The deeper strata experiences little to no pressure dissipation due to the short loading period and hence no further compaction. As the ice melts away, both vertical stress and fluid pressure reduces throughout the succession leaving only a lasting over-compaction imprint on the upper few hundred meters where some pressure dissipation occurred. Such glacial effects complicates establishment of normal compaction trends (e.g. for porosity and velocity), because such trends implicitly rely on monotonously increasing maximum effective stress with depth.

According to Nielsen et al. (2015), the Tertiary succession contains various clay types giving some uncertainty in what the general permeability is. In this paper an average permeability of $10^{-5}mD$ ($10nD$) was found to produce acceptable results during modeling of transient pressure development to match observed pressure and logged porosity. This is similar to assumed permeability for the equivalent succession studied in a pressure modeling study near the Judy Field (Swarbrick et al. 2005). Comparing this permeability with the trends of Mondol et al. (2008) adjusted to the reduced porosity range found in the normal compaction trend in the area, the value compares to within the variation for smectite - kaolinite admixtures, broadly consistent with the mineralogy of the sealing succession (Fig. 10; Nielsen et al. 2015). Neuzil (1994) estimates similar ranges of permeability for a selection of North American clay formations based on laboratory experiments and argue that these apply to basin scale conditions based on inverse analysis of flow systems.

The purpose of estimating permeability and compressibility discussed above is to estimate the pressure diffusivity (equation 3) required for estimating the transient pressure development originating from rapid deposition. Compressibility and permeability will reduce as compaction progresses. However, as these parameters are in the denominator and enumerator of the diffusivity (equations 3, 2), the change of diffusivity with burial is likely to be rather subdued in the effective stress interval of interest. The diffusivity is therefore approximated by a constant in this paper adjusted to allow the below forward modeling of pressure to end up at observed present-day porosity and pressure. The diffusivity may thus be described by a compressibility of $c_b = 2 \cdot 10^{-8} Pa^{-1}$, a permeability of $K = 10^{-5}mD = 10nD$, a viscosity of $\mu = 10^{-3}Pas$, and a porosity of $\phi = 0.3$. These values correspond roughly to a 70% smectite, 30% kaolinite mix at $\sigma'_v \sim 5MPa$ (Figs 8, and 10). This is not to say that this is the actual clay mineral composition.

This allows forward modeling of the interaction between sedimentation loading, pressure build-up and compaction for comparison with pressure data and the Eaton analysis as exemplified below.

Forward pressure modeling

Assuming equation 7 to adequately describe the compaction of sediments, the burial history is modeled in a forward manner such that present-day thicknesses and poros-

ity are obtained. The approach is to subdivide the succession into as many layer as required to resolve significant variation in burial rates and differences in lithology and associated porosity. Variation in parameters ϕ_0 and a of equation 7 for each layer have been done to optimize the match to the present porosity (example in Fig. 11).

For each layer in reverse order (numbered from top to bottom in well) the modeling procedure is:

• Subdivide the depositional period into time-steps (here chosen to be 200,000 years) where loading per time-step is obtained from equation 16 in the appendix.

• During deposition hydrostatic conditions are assumed for the top layer (only) such that a simple relationship between depth and effective stress is maintained in the top layer.

• Pressure in the previously deposited (deeper) layers is then perturbed (increased) by the added load (effective stress increase as given by Terzaghi's equation). Then the dissipation of this pressure anomaly added to the anomaly inherited from previous time-steps is calculated. Pressure dissipation is calculated using a simple finite-difference (FD) numerical approximation to equation 3 using the diffusivity discussed above. For a stable FD solution, minor sub-steps may be invoked.

• The depth increment is $1m$ and a 2-D array with time in x direction and depth (below mudline) in the vertical collects the pressure profiles for all time steps.

• 2-D arrays keep track of overpressure and layer depths and are updated for each time-step.

While the pressure diffussivity is assumed constant as discussed in the previous section, variation in modeled overpressure originates from the thickness of the sealing succession and the loading rate as it changes through time. Therefore, details of the chronostratigraphy and porosity variation of the Cenozoic succession in the modeled wells (to obtain the load) are required;- the more the better. Unfortunately biostratigraphic work in the chalk overburden is often neglected in many wells of which the forward modeled wells in this paper are useful exceptions.

It is noted that water depth is not important, as the key driver for compaction is effective stress,- not absolute stress. Water depth is added posterior to compaction calculations.

Forward modeling of deposition at the Bertel-1 well location using these relations shows a slight build-up of overpressure around $30Ma$. Still, main overpressure to develop in the last $10Ma$ reaching just over $14MPa$ at top chalk level in accordance with observations in the area (Fig. 12). The main pressure-build up coincided with accelerated Neogene deposition and estimated rapidly reducing water depth reaching around $65m$ at present (palaeo depths modified from Gemmer et al. 2002). The resulting modeled vertical pressure profile shows a good match to the Eaton analysis (Fig. 5). However, the simulated dissipation processes inevitably result in a smooth pressure profile unlike the raw unfiltered Eaton estimate that also contain

effects unrelated to pressure as discussed previously.

If the permeability is increased by a factor of 10, the maximum overpressure would only reach $\sim 4MPa$, and result in more compaction and thus increasing present water depth by about $200m$ (Fig. 13). Effective stress development through time as given by the Terzaghi equation (equation 6) is portrayed in the lower plot of Fig. 12. A local maximum develops at top overpressure along with a considerable increase in effective stress in the upper part of the overpressured section as opposed to at the base (Fig. 14). The modeled rather monotonous increase in effective stress through time, and the match to pressure observations suggests that the premise for doing Eaton analysis holds for the Cenozoic,- unlike for the Jurassic (Fig. 14).

A similar analysis is shown for the Nana-1 well (Figs 1, 15). This well is located in the southern part of the Danish Central Graben area, and the same diffusivity as for Bertel-1 was applied. The somewhat lower overpressure of around $8MPa$ shown by MDT data is matched fairly well with the model. The main phase of overpressure build-up within the last 10Ma is broadly similar to what occurs to the North but the early weak pressure build-up at around $30Ma$ is missing to the South.

A map compiling overpressure estimates originating from the Eaton analyses, forward modeling and empirical estimates at top Chalk level in the area around Bertel-1 is shown in Fig. 16. The map is not explicitly using overpressure observations (white boxes with red numbers) but rely on the predictive tools, supplemented with minor edits. Contouring is supported by an empirical correlation of pressure data points to the depth of top over-pressure (a smooth surface representing the load), and the thickness of the interval top overpressure - top chalk interval (representing the sealing succession). Hydrocarbon effects (buoyancy forces) have been omitted as for the data in Table 1. However, in the case of the South Arne field (the Baron 1 and 2 and the Rigs-1,2 and 4 wells), the water phase pressure data are still affected by oil phase pressures in complex manner akin to the so-called perched water mechanism discussed in greater detail in Vejbæk et al (2015).

In the northeast corner of the map, anomalously low overpressure broadly follows the extent of Paleocene sands extending from the Northeast into the study area, resting on top of the Chalk and partially draining pressures,- often referred to as the "Siri fairway" (e.g. Hamberg et al. 2005). Interestingly these sands do not affect the pressure in wells quite close by, such as the Iris-1 well. That these sands may partially drain pressure out of the area to the Northeast is corroborated by observation of injectite structures associated with the correlative sands to the Northeast in a near hydrostatic pressure area (Hamberg et al. 2007).

General permeability in the chalk is higher than what is assumed for the Paleogene sealing succession but apparently still too low to provide significant lateral pressure dissipation. Tilted fluid contacts are usually observed in chalk fields primarily (but not exclusively) attributed to lateral pressure variation in the water leg, often referred to as flow (e.g Dennis et al. 2005). However, the efficacy of the flow is clearly insignificant as equilibrated (flat) contacts in North Sea chalk fields are hard to find. Geological time-scale simulation of the filling and re-migration process

of several chalk oil fields in the general study area suggests increasing rather than decreasing pressure gradients in the studied chalk fields in Neogene times and predicts equilibration time that compares to or exceeds the main overpressure build-up time as presented in this paper (e.g. Vejbæk et al. 2005, Vejbæk et al. 2015).

Two wells have pressure significantly higher than predicted by the map. They are the Olaf-1 well ($\sim 10km$ south-west of the Bertel-1 well) having $18MPa$ above hydrostatic instead of the predicted $13.5MPa$,- and the Nora-1 well (southeast corner of the map) where $15.5MPa$ is observed as opposed to the predicted $12MPa$. However, both of these wells penetrate major faults in the chalk off-setting the base of the chalk, thus likely allowing partial access for the much higher pressures in the Jurassic. Similarly, observation of initial overpressure in the upper chalk in the order of $20MPa$ in the Valhall Field just North of the Norwegian-Danish sector boundary is deemed indicative of a connection to higher pressure in the Jurassic (e.g. Zoback and Zinke 2002).

Jurassic overpressure

If the general plastic compressibility trend for the Tertiary also applies to the Jurassic, it would be reduced by a third to a fifth of the compressibility of the Tertiary (Fig. 8). Recalling the significance of compressibility and permeability for pressure diffusivity in equation 3, much lower permeability is required to sustain the much larger overpressure observed in the Jurassic if it is generated by dis-equilibrium compaction (e.g. Fig. 2). As the pressure is close to the fracture pressure in Amalie-1, one-dimensional dis-equilibrium compaction would require a perfect seal to ensure little or no pressure dissipation since the time of deposition in the Jurassic (Fig. 2; cf Nordgård Bolås et al. 2004). The (local) pressure gradient in the upper part of the Jurassic in this well is close to a water gradient suggesting that permeability is not in the nano-Darcy range. Dis-equilibrium compaction is therefore considered an unlikely mechanism for generating the overpressures in the Jurassic. This has also been proposed by several authors who suggest volume expansion (and high compressibility) associated with the generation of hydrocarbons from the rich Upper Jurassic source rocks to generate overpressure causing un-loading (e.g. Ward et al. 1994, Osborne and Swarbrick 1997). As an alternative, stress in-sensitive diagenetic processes in the clay has been suggested by Nordgård Bolås et al. (2004) to generate overpressure and hence unloading. They also noticed a discrepancy between porosity and overpressure in the pre-Cretaceous of the Norwegian North Sea. Contributions from dis-equilibrium compaction may still play a minor role, and have been suggested as the main mechanism for the pre-Cretaceous pressure at the Judy Field area in British North Sea North-west of the study area of this paper but there the overpressure was only moderate (not close to the fracture pressure; Swarbrick et al. 2000).

Un-loading means that present effective stress has been reduced compared to before the onset of unloading, whether it be a consequence of hydrocarbon generation

or diagenetic processes. Unloading makes Eaton type analysis, or similar methods relying on the degree of compaction, unsuitable for estimating overpressure as simple correlation between pressure and degree of compaction is lost.

Jurassic overpressure levels have been recorded in many wells in the study area, ranging from about $18MPa$ (Baron-2, Fig. 18), to around $47MPa$ above hydrostatic. If hydrocarbon generation is the main reason for over-pressuring, pressures likely reflect variation in richness (TOC, HI) and maturity of the source rock. The control by richness is difficult to test without a detailed spatial mapping of the same. However, broad variation in richness and maturity is available for the general Danish Central Graben area (Damtoft et al. 1992). Alternatively if diagenetic processes are the main cause (Nordgård Bolås et al. 2004), temperature could be the main controlling factor. The maturity and temperature are largely controlled by burial depth, which can easily be compared to a top Jurassic depth map. This level is ideal, as the richest source rock, the Bo Member or Hot unit closely follows below this surface and in the westernmost and southernmost parts of the Danish Central Graben maturity and quality of the main Upper Jurassic source rock drops (Damtoft et al 1992, Petersen et al. 2010). South of the Nana-1 well it is even immature.

A cross-plot of depth to top Jurassic versus magnitude of upper Jurassic overpressure shows an excellent correlation (Fig. 17). The relationship is:

$$\Delta P = 0.0294 \cdot z - 80.44 \tag{12}$$

yielding values in MPa with a standard deviation of $1.5MPa$, if Bertel-1 is omitted from the trend. The resulting map of Upper Jurassic overpressure uses this correlation to the measured pressures, and should therefore be used with great caution due to it's empirical nature (Fig. 18). Green polygons show areas where pressure is constrained by the fracture gradient (in the order of 2 to $3MPa$ below σ_v), and pink polygons show areas where the overpressure difference between the Upper Jurassic and the Upper Cretaceous is negligible exemplified by the Saxo-1 and Wessel-1 wells. At these wells, the Upper Jurassic is thin and/or immature concerning hydrocarbon generation, which also appears to apply to the anomalous Bertel-1 well (Petersen et al. 2016). Conversely, the Olaf-1 well, that was suggested to have elevated overpressure at top Chalk level due to partial communication to the Jurassic, is seen to sit at the edge of a high Jurassic pressure area (Fig. 18).

Conclusions

A three-fold subdivision of the pressure regime in the Jurassic to recent sedimentary succession in the northern Danish Central Graben area has been applied in line with previous studies (e.g. Hunt 1990, Powley 1990; Ward et al. 1994). The uppermost hydrostatic pressure succession down to around the mid-Miocene at $\sim 1200m$ depth in the North and $\sim 700m$ in the South cannot build significant overpressure, which may be due to intercalations of slightly coarser clastic material as suggested by the

low-angle progradational bed geometries seen in the seismic in accordance with the lithological description (e.g. Rasmussen 2005, Rasmussen et al. 2013, Schiøler et al 2007).

The Upper Cretaceous to mid-Miocene succession has medium-high overpressure consistent with a dis-equilibrium compaction mechanism corroborated by consolidation analysis (Eaton method), forward modeling and direct pressure observations at Upper Chalk level. As required for the Eaton analysis to work, maximum effective stress is achieved in recent times, and pressure levels are in general consistent with the magnitude of rapid Neogene loading as has already been shown by Japsen (1999). Earlier studies has favored rather confined stratigraphic intervals to provide the seal for the mid-Miocene to Upper Cretaceous pressure cell (e.g. Hunt 1990). In this study this entire succession is proposed to be sealing as corroborated by both the Eaton analysis and the forward modeling. A similar modeling study around the Judy Field, around 200km north of the area studied here also assumed most of the Chalk overburden to be sealing at a similar permeability level, - but including more recent parts of the succession than the mid Miocene (Swarbrick et al. (2005). The Chalk is not encompassed by the Eaton calibration presented here and would require a separate calibration. However, Japsen (1998) showed that velocity variation within the chalk could be used to derive anomalous consolidation trends, including unloading by uplift or dis-equilibrium compaction by overpressure.

Earlier studies on forward modeling of the Upper Cretaceous to mid-Miocene pressure used similar permeability ($10^{-5}mD = 10nanoD$; Vejbæk 2008; Swarbrick et al. 2005). However, Vejbæk (2008) used a somewhat higher plastic compressibility for the diffusivity estimate in the same area. In that study a semi-analytical solution to equation 3 was applied, and the compressibility was 6 to 7 times higher. Additionally higher viscosity was deployed. This results in a somewhat slower dissipation rate in the old study, which is seen as slightly higher pressures. The updated calculation presented in the paper gains from a better (shallower) definition of top overpressure, and plastic compressibility as constrained by the Eaton analysis.

The Eaton calibration is here exploited to obtain parameters for forward modeling of the observed pressure. The benefits of doing forward modeling include validating the implicitly assumed dis-equilibirium compaction mechanism: Is the assumed loading process able to generate the observed overpressure? Are the required sealing properties reasonable? Good matches to observed pressure can be achieved with the method. Valid observations include down-hole pressure measurements that can be assigned to specific depths. Thus, mud-weights are not valid unless inflow, including the depth where it occurred, has been observed. However, a detailed geomechanical analysis may allow valid information on the pressure to be extracted from mud-weights in some cases.

In addition the forward modeling can help filter out lithological effects from the Eaton pressure estimate, and obviously provide information on the timing of the pressure build-up.

High to extreme Jurassic pressure is interpreted to be generated by unloading.

This means that bulk compressibility would be dominantly elastic, thus challenging the longevity of overpressure. However, Muggeridge et al. (2005) discusses that the presence of hydrocarbons may lower compressibility sufficiently for overpressure to persist in geological time-scales. The required duration of overpressure in the Jurassic is less well-constrained than for the lower Tertiary. However, basin-modeling suggests maturation of the main source rocks to occur coeval with Neogene deposition, reducing requirements for small diffusivity, and making the high Jurassic overpressure possibly even more recent than for the lower Tertiary (e.g. Damtoft et al-. 1992, Pletsch et al. 2010).

Acknowledgements

I would like to thank Hess Denmark for permission to present this work. Gratitude is owed to Finn Mørk, GEUS, for compiling the pressure data as part of the CRETSYS project.

References

Athy, L. F. 1930. Density, porosity and compaction of sedimentary rocks. *American Association of Petroleum Geologists Bulletin*, **14**, 1-24.

Bendixen, C., Lamb, R., Huuse, M. Boldreel, L., Jensen, J. B. and Clausen, O. R. 2018. Evidence for a grounded ice sheet in the central North Sea during the early Middle Pleistocene Donian Glaciation. *Journal of the Geological Society*, **175**, 291–307.

Bowers, G. L. 1995. Pore pressure estimation from velocity data; accounting for overpressure mechanisms besides undercompaction. *SPE Drilling and Completions* , June, SPE 27488, 89–95.

Dake, L. P. 1978, *Fundamentals of reservoir engineering.* Amsterdam, Elsevier, Developments in Petroleum Science 8, 443 p.

Damtoft, K., Nielsen, L. H., Johannessen, P. N., Thomsen, E. and Andersen, P. R. 1992. Hydrocarbon plays of the Danish Central Trough. *In:* A. M. Spencer (ed) *Generation, Accumulation and Production of Europe's Hydrocarbons II.* Special Publication of the European Association of Petroleum Geoscientists, **2**, Springer Verlag, Berlin.

Dennis, H., Bergmo P. and Holt, T. 2005. Tilted oil-water contacts: modelling effects of aquifer heterogeneity. *In:* Doré , A. G. and Vining, B. A. (eds) *Petroleum Geology: North-West Europe and Global Perspectives—Proceedings of the* 6^{th} *Petroleum Geology Conference* , Petroleum Geology Conferences Ltd. Published by the Geological Society, London. 145 – 158.

Eaton, B. A. 1975. The equation for geopressure prediction from well logs. *SPE Annual Technical Conference and Exhibition*, Paper 5544.

Fabricius, I. L. 2007. Chalk: composition, diagenesis and physical properties. *Bulletin of the Geological Society of Denmark*, **55**, 97 - 128.

Fabricius, I. L. and Borre, M. K. 2007. Stylolites, porosity, depositional texture, and silicates in chalk facies sediments. Ontong Java Plateau – Gorm and Tyra fields, North Sea. *Sedimentology,* **54**, 183 – 205.

Gemmer, L., Nielsen, S. B., Huuse, M. and Lykke-Andersen, H. 2002. Post-mid-Cretaceous eastern North Sea evolution inferred from 3D thermo-mechanical modelling. *Tectonophysics,* **350**, 315 – 342.

Hamberg, L., Dam, G., Wilhelmson, C. and Ottesen, T. G. 2005. Paleocene deep-marine sandstone plays in the Siri Canyon, offshore Denmark–southern Norway. *In:* Doré , A. G. and Vining, B. A. (eds) *Petroleum Geology: North-West Europe and Global Perspectives—Proceedings of the* 6^{th} *Petroleum Geology Conference* , Petroleum Geology Conferences Ltd. Published by the Geological Society, London. 1185–1198.

Hamberg, L., Jepsen, A.-M., Ter Borch, N., Dam, G., Engkilde, M. K. and Svendsen, J. B. 2007. Mounded structures of injected sandstones in deep-marine Paleocene reservoirs, Cecilie field, Denmark. *In:* A. Hurst & J. Cartwright, (eds) *Sand injectites: Implications for hydrocarbon exploration and production.* American Association of Petroleum Geologists, Memoir, **87**, 69-79.

Hermanrud, C. and Undertun, O. 2019. Resolution limits of fluid overpressures from mineralogy, porosity, and sonic velocity variations in North Sea mudrocks. *American Association of Petroleum Geologists Bulletin*, **103**, 2665 -2695.

Hunt, J. M., 1990. Generation and migration of petroleum from abnormally pressured fluid compartments. *American Association of Petroleum Geologists Bulletin*, **74**, 1–12.

Huuse, M. and Lykke-Andersen, H. 2000. Overdeepened Quaternary valleys in the eastern Danish North Sea: morphology and origin. *Quaternary Science Reviews* **19**, 1233-1253.

Japsen, P. 1993. Influence of lithology and neogene uplift on seismic velocities in Denmark: Implications for depth conversion of maps. *American Association of Petroleum Geologists Bulletin* **77**, 194-211.

Japsen, P. 1998. Regional velocity-depth anomalies, North Sea Chalk; a record of overpressure and Neogene uplift and erosion. *American Association of Petroleum Geologists Bulletin,* **82**, 2031-2074.

Japsen, P. 1999. Overpressured Cenozoic shale mapped from velocity anomalies relative to a baseline for marine shale, North Sea. *Petroleum Geoscience,* **5**, 321-336.

Kristensen, T. B. and Huuse, M. 2012. Multistage erosion and infill of buried Pleistocene tunnel valleys and associated seismic velocity effects. *In:* Huuse, M., Redfern, J., Le Heron, D. P., Dixon, R. J., Moscariello, A. and Craig, J. (eds): 2012. *Glaciogenic Reservoirs and Hydrocarbon Systems.* Geological Society, London, Special Publications, **368**, 159–172.

Mavko, G., Mukerji, T. and Dvorkin, J. 1998. *The Rock Physics handbook.* Cambridge University Press. 329 p.

Medvedev, S., Hartz, E. H., Schmid, D. W., Zakariassen, E. and Varhaug, P. 2020. Influence of glaciations on North Sea petroleum systems. *In:* Patruno, S., Archer, S. G., Chiarella, D., Howell, J. A., Jackson, C. A.-L. and Kombrink, H. (eds): *Cross-Border Themes in Petroleum Geology I: The North Sea.* Geological Society, London, Special Publications, 494, 20 p.

Mondol, N. H., Bjørlykke, K., and Jahren, J. 2008. Experimental compaction of clays: relationship between permeability and petrophysical properties in mudstones. *Petroleum Geoscience*, **14**, 319–337.

Muggeridge, A. Abacioglu, Y., England, W., and Smalley, C. 2005. The rate of pressure dissipation from abnormally pressured compartments: *American Association of Petroleum Geologists Bulletin*, **89**, 61– 80.

Neuzil, C. E., 1994. How permeable are clays and shales?: *Water Resource Research* v. 30, p. 145– 150.

Nielsen, O. B., Rasmussen, E. S., and Thyberg, B. I. 2015. Distribution of clay minerals in the northern North Sea basin during the paleogene and Neogene: a result of source-area geology and sorting processes.*Journal of Sedimentary Research*, **85**, 562–581.

Nordgård Bolås, H. M., Hermanrud, C., and Teige, G. M. G. 2004. Origin of overpressures in shales: Constraints from basin modeling. *American Association of Petroleum Geologists Bulletin,* **88**, 193–211.

Nordgård Bolås, H. M., Hermanrud, C., Schutter, T.A., and Teige, G. M. G. 2008. Is stress insensitive chemical compaction responsible for high overpressures in deeply buried North Sea chalks?*Marine and Petroleum Geology*, **25**, 565-587.

Osborne, M. J., and R. E. Swarbrick, 1997, Mechanisms for generating overpressure in sedimentary basins, a re-evaluation: *American Association of Petroleum Geologists Bulletin,* **81**, 1023–1041.

Petersen, H. I., Hertle, M., Juhasz, A. and Krabbe H. 2016. Oil family typing, biodegradation and source rock affinity of liquid petroleum in the Danish North Sea. *Journal of Petroleum Geology* **39**, July, 247-268.

Petersen, H. I., Nytoft, H. P., Vosgerau, H., Andersen, C., Bojesen-Koefoed, J. A. and Mathiesen, A. 2010. Source rock quality and maturity and oil types in the NW Danish Central Graben: implications for petroleum prospectivity evaluation in an Upper Jurassic sandstone play area. In: Vining, B. A. and Pickering, S. C. (eds): *Petroleum Geology: From Mature Basins to New Frontiers*, Proceedings of the 7^{th} Petroleum Geology Conference, 1 – 13. Petroleum Geology Conferences Ltd. Published by the Geological Society, London.

Pletsch, T., Appel, J., Botor, D., Clayton, C.J., Duin, E.J.T., Faber, E., Gorecki, W., Kombrink, H., Kosakowski, P., Kuper, G., Kus, J., Lutz, R., Mathiesen, A., Ostertag-Henning, C., Papiernek, B. and Van Bergen, F., 2010. Petroleum Generation and Migration. In: Doornenbal, J.C. and Stevenson, A.G. (eds): *Petroleum*

Geological Atlas of the Southern Permian Basin Area. EAGE Publications b.v. (Houten): 225-253.

Powley, D. E., 1990. Pressures and hydrogeology in petroleum basins: *Earth-Science Reviews*, **29**, 215–226.

Rasmussen, E. S. 2005. The geology of the upper Middle–Upper Miocene Gram Formation in the Danish area. *Palaeotos*, **7**, 5-18.

Rasmussen, E. S. 2013. Cenozoic structures in the eastern North Sea Basin — A case for salt tectonics: Discussion. *Tectonophysics*, **601**, 226–233.

Schiøler, P., Andsbjerg, J., Clausen, O. R., Dam, G., Dybkjær, K., Hamberg, L., Heilmann-Clausen, C., Johannessen, E. P., Kristensen, L. E., Prince, I., and Rasmussen, J. A. 2007. Lithostratigraphy of the Palaeogene – Lower Neogene succession of the Danish North Sea. *Geological Survey of Denmark and Greenland Bulletin.* **12**, 77 p.

Sclater, J. G. and Christie, P. A. F. 1980. Continental stretching: an explanation of the post-mid-Cretaceous subsidence of the Central North Sea basin. - *Journal of Geophysical Research*, **85, b7**, 3711-3739.

Swarbrick, R.E., Osborne, M.J., Grunberger, D., Yardley, G.S., Macleod, G., Aplin, A.C. Larter, S.R., Knight, I. and Auld, H.A. 2000. Integrated study of the Judy Field (Block 30/7a) - an overpressured Central North Sea oil/gas field. *Marine and Petroleum Geology,* **17**, 993–1010.

Swarbrick, R. E., Seldon, B. and Mallon, A. J. 2005. Modelling the Central North Sea pressure history. In: Doré , A. G. & Vining, B. A. (eds) *Petroleum Geology: North-West Europe and Global Perspectives*, Proceedings of the 6^{th} Petroleum Geology Conference, 1237–1245. Petroleum Geology Conferences Ltd. Published by the Geological Society, London.

Vejbæk, O.V. 2008. Disequilibrium compaction as the cause for Cretaceous - Paleogene overpressures in the Danish North Sea. *American Association of Petroleum Geologists Bulletin*, **92**, 165-180.

Vejbæk, O. V., Frykman, P. Bech, N. and Nielsen, C. M. 2005. The history of hydrocarbon filling of Danish chalk fields. *In:* Doré, A. G. and Vining, B. (eds). *Petroleum Geology: North-West Europe and Global Perspectives - Proceedings of the* 6^{th} *Petroleum Geology Conference*, 1331-1345. Petroleum Geology Conferences Ltd. Published by the Geological Society, London.

Vejbæk, O. V., Bech, N., Christensen, S.A., Høie, A., If, F., Kosco, K., Schiøtt, C. R. and White, G. 2015. Modelling un-equilibrated oil saturations in a chalk reservoir, the South Arne Field case. *Society of Petroleum Engineers* SPE 174085, 16p.

Ward, C. D., Coghill, K. and Broussard, M. D. 1994. The application of petrophysical data to improve pore and fracture pressure determination in North Sea Central Graben HPHT wells. *Society of Petroleum Engineers* SPE 28297, 53-68.

Zoback, M. D. and Zinke, J. C. 2002. Production-induced normal faulting in the Valhall and Ekofisk oil fields. *Pure and Applied Geophysics* , **159**, 403-420.

APPENDIX

Forward modeling of pressure is based on the assumption that equation 7 adequately describes the compaction of the sediments.

The start procedure is to estimate the amount of solids in each layer (n) using present depths and average porosity ($-\phi_{av,n}$) from log data:

$$S_n = (1 - \phi_{av,n}) \cdot (z_{2,n} - z_{1,n}) \tag{13}$$

To find the maximum depth achieved during sedimentation of a layer, we need to find the z at each time step for which:

$$S_n = \int_0^{z_2} (1 - \phi_0 e^{-a\sigma'(z)}) \partial z \tag{14}$$

where ϕ_0 is porosity at zero effective stress ($\sigma'(z)$), and a the porosity decay constant. This equation describes accumulated solids during the sedimentation. A solution is:

$$S_n = z \cdot (1 - \phi_{mean}) = z \cdot (1 - \frac{\phi_0}{-a \cdot \sigma'(z)} (e^{-a\sigma'(z)} - 1)) \tag{15}$$

which can be solved for $\sigma'(z)$, and thus for z if $\sigma'(z)$ is known. Isolating $\sigma'(z)$ is not straight forward, so an iterative approach can be applied. A simpler approach is to integrate equation 14 numerically, which allows the function $\sigma'(z)$ to have more complex shapes than the commonly assumed linear increase with z, as will be the case when overpressure builds up.

During the sedimentation period for a specific layer, hydrostatic pressure is assumed to be maintained for that layer, so that the sedimentation velocity can be calculated from:

$$v_0 = \frac{1}{(1 - \phi_0)\Delta t} \left[\Delta\sigma'(z) + \frac{\phi_0}{a} (e^{-a\sigma'(z_2)} - 1) \right] \tag{16}$$

it is noted that $\Delta\sigma'(z) = \sigma'(z_2) - \sigma'(z_1)$, where we assume $\sigma'(z_1) = 0$.

During sedimentation, the $\sigma'(z,t)$ function (giving the subsidence curve shape within the sedimentation period) is found from:

$$t = \frac{1}{v_0(1 - \phi_0)} \left[\sigma'(z) + \frac{\phi_0}{a} (e^{-a\sigma'(z_2)} - 1) \right] \tag{17}$$

Iteration needs to be applied to find $\sigma'(z)$ varying between 0 and $\sigma'(z_2)$ as function of t.

During burial beyond the sedimentation period (when the layer is buried deeper), there are analytical solutions for burial at hydrostatic conditions similar to equation but due to non-linearity caused by overpressure, we evaluate:

$$S_n = \int_{z_1}^{z_2} (1 - \phi_0 e^{-a\sigma'(z)}) \partial z \tag{18}$$

numerically to find the base through time.

Pressure dissipation (equation 3) may be solved by simple explicit finite difference (FD) methods. Loading (perturbation) is applied in linear segments of $200ka$ but time step during FD iteration is only 200 years to ensure numerical stability.

Well	Forward modeling	Eaton Estimation	Chalk data	Jurassic data
Amalie-1		*		4158
Augusta-1			2973	
Baron-1,2			2832	3117
Bertel-1	*	*		4722
Diamant-1	*	*		3798
Gert-1			3297	4867
Gwen-2		*		4182
Hejre-2		*		5360
Iris-1			3110	3916
Jette-1		*		4190
Kim-1		*		4578
Lone-1			3292	3472
Mona-1		*	3174	4260
Nana-1	*		2213	
Nora-1			[3]2582	
Ofelia-1		*		
Olaf-1			[3]3048	
Rigs-1		*	2795	
Rigs-2	*		2850	
Rigs-4	*	*	2779	
Saxo-1		*	[2]2500	3042
Solsort-1			[1]3025	
Solsort-2			[1]3020	
Spurv-1			3240	
Svane-1				5347
Tabita-1			2999	
Wessel-1		*	[2]2780	3002

Table 1: Well data base of pressure points in the Chalk and Jurassic listed as representative depths in meters (last two columns). If sufficient information has been available, estimation by Eaton analysis and forward modeling has been applied (stars in second and third columns). Points marked [1] are from sandy layers resting on the chalk, points marked [2] are from sandy layers in contact with the base of the chalk, and [3] are pressure points at major faults crossing the base Chalk.

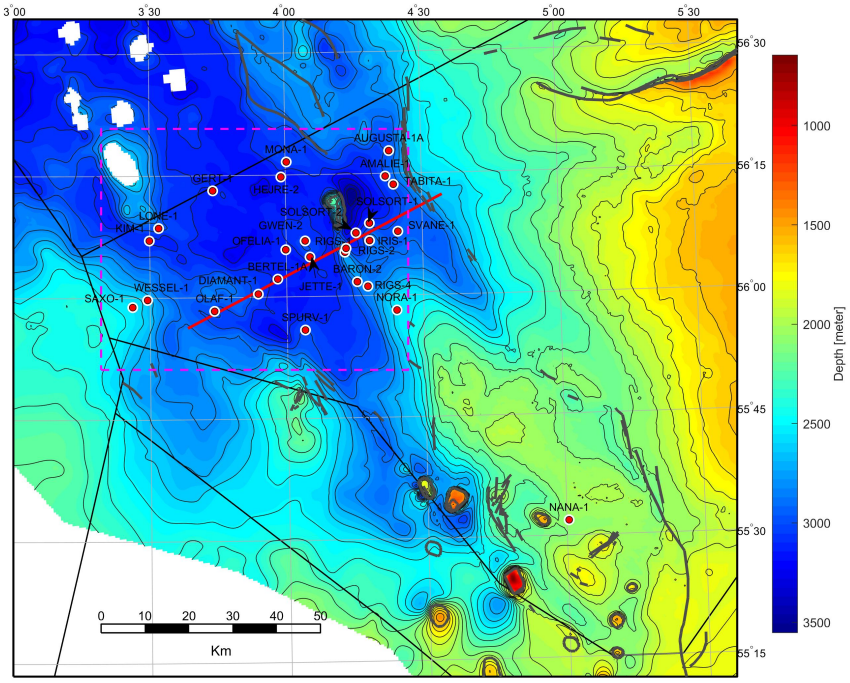

Figure 1: Top chalk depth structure map, (c.i. $100m$). Thick black lines are national sector boundaries, gray lines are major faults, Red dots are locations of selected wells mentioned in the text, and the thick red line shows the location of the seismic line in Fig. 7. Pink dashed line shows location of the maps in Figs. 16 and 18.

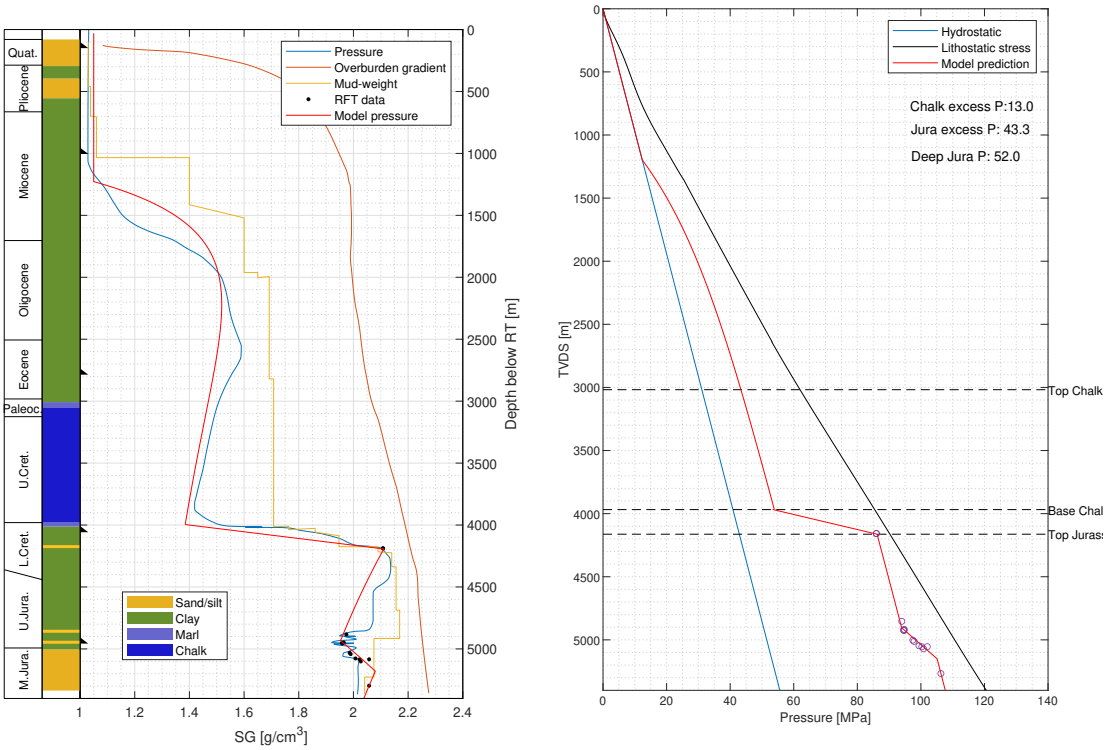

Figure 2: The pressure distribution in the Amalie-1 well is a good example of a pressure profile from well reports normalized to equivalent mud weight (redrawn from report, left). The right plot shows absolute pressure estimated by support from neighboring wells, Eaton analysis and forward modeling. Pressure measurements (circles) document a further increase at around $5km$ depth. The pressure profile in the right plot is superimposed in the left plot in red with the operators estimate in blue. See Fig. 1 for location.

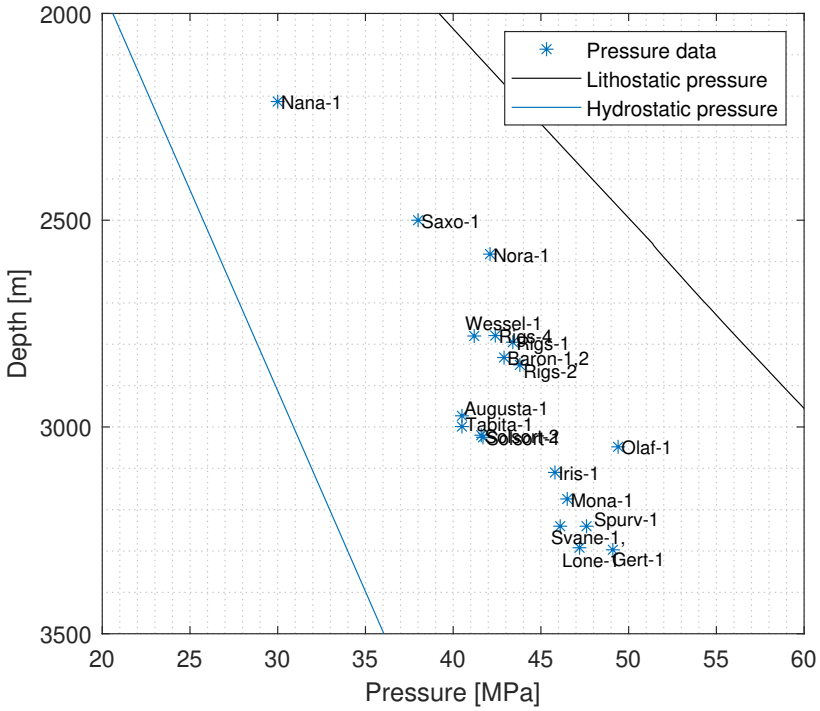

Figure 3: Pressure points from the chalk and juxtaposed layers (see Table 1) simplified to a single point per well. The observed variation in overpressure is mainly attributed to variation in Cenozoic burial history.

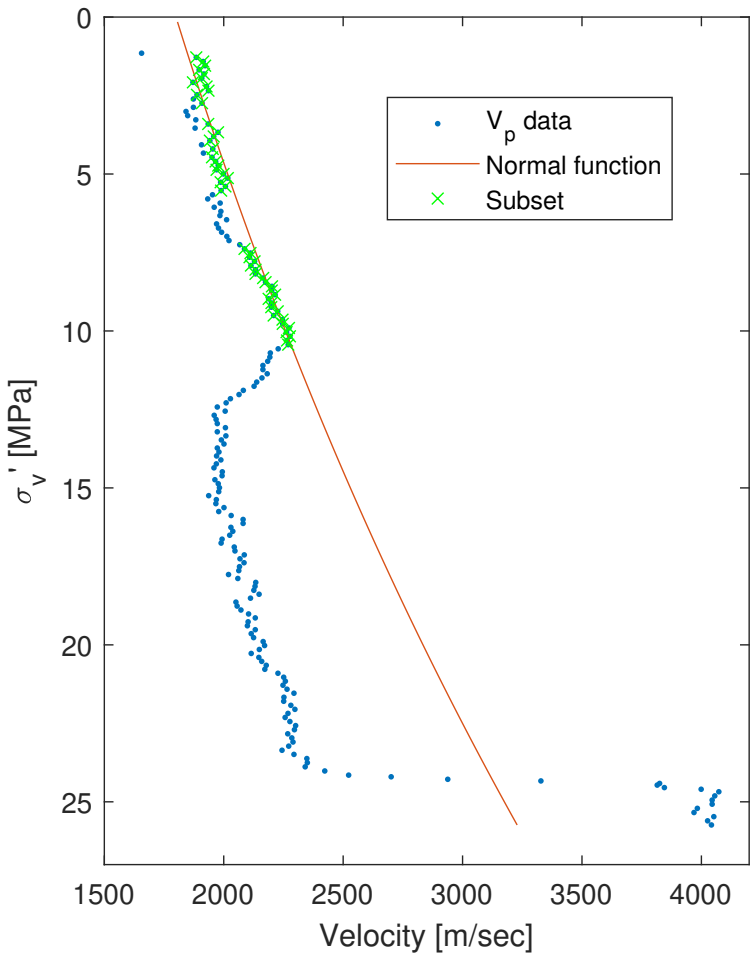

Figure 4: Interval velocity from vertical seismic profiling in the Rigs-4 well plotted against effective stress assuming hydrostatic conditions. A trend is defined using a subset of clay dominated data points (crosses) up to around $10MPa$ with a standard deviation of $\pm 27m/sec$. The clear reduction in velocity above this stress level is assumed to mainly reflect overpressuring.

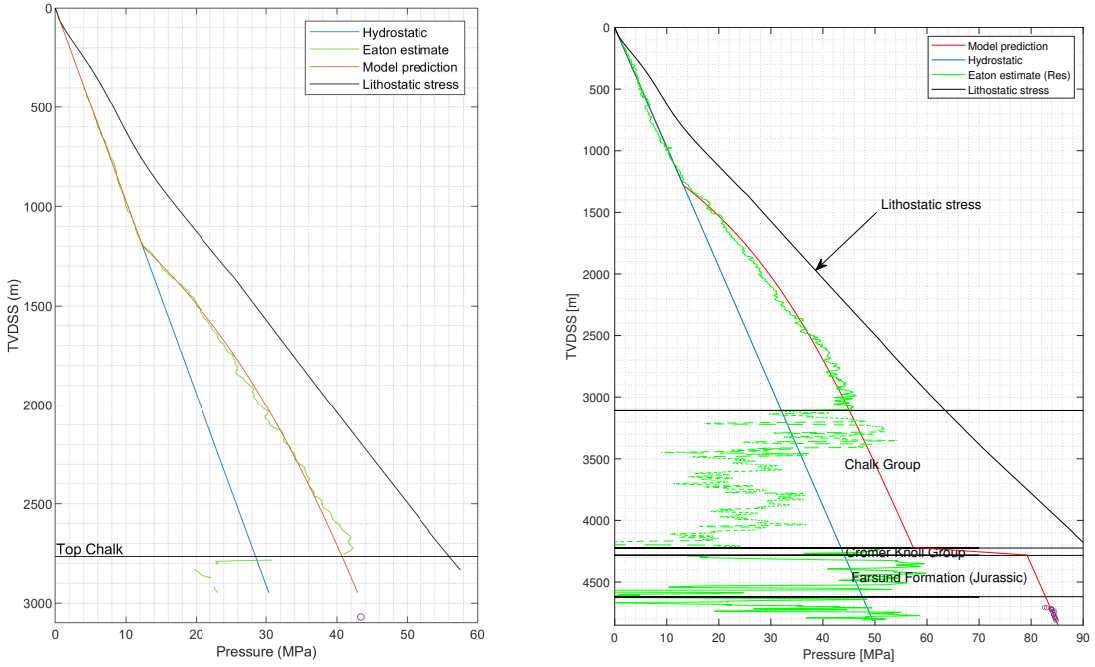

Figure 5: Pressure estimates using the Eaton approach (green curves) for the Rigs-4 well based in sonic data (left) and the Bertel-1 well based on resistivity (right). Measured pressure is available for both wells (circles). For Bertel a pressure of $83.9MPa$was measured in the Jurassic at $4722m$ vastly exceeding both Eaton and forward modeling estimates (compare Table 1 and Fig. 18). Forward modelled pressure for both wells is shown in red, with suggested extension into the Jurassic in Bertel-1. Location is shown in Fig. 1. The Eaton curves are dashed in the Chalk, as the calibration applies to overburden shale and not chalk.

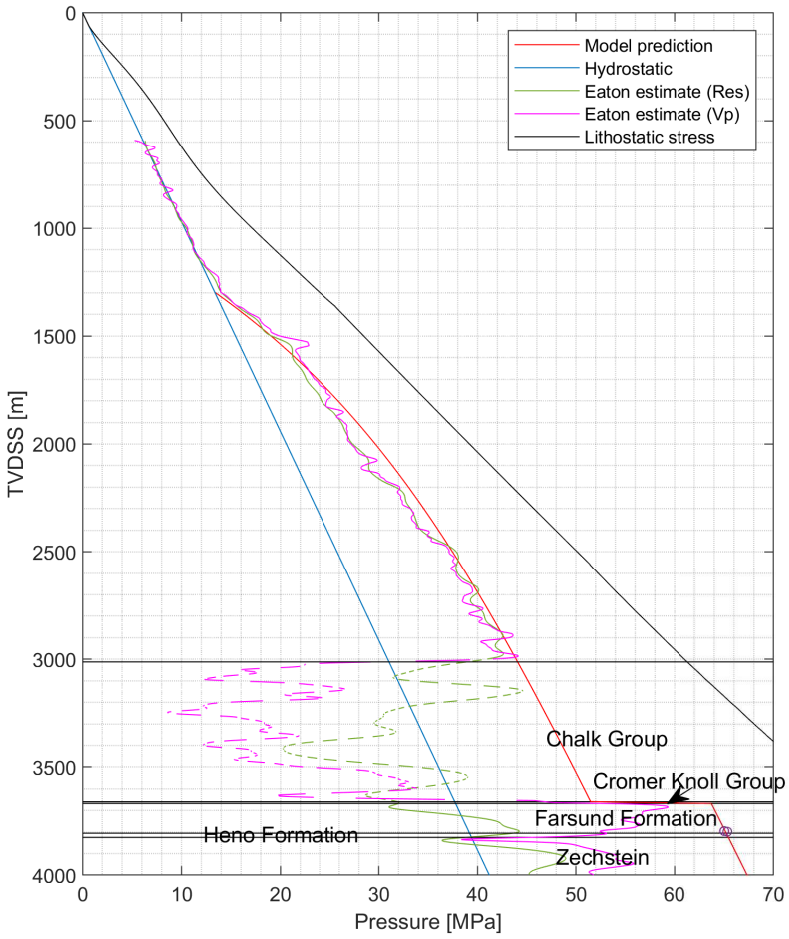

Figure 6: Overpressure estimate using the Eaton method based on resistivity and velocity logs for Diamant-1. The Eaton estimates are in green and pink, and forward modeling in red with conjectured extension into the Jurassic. The Eaton curves are dashed in the Chalk, as the calibration applies to overburden shale and not chalk. Circles are pressure measurements.

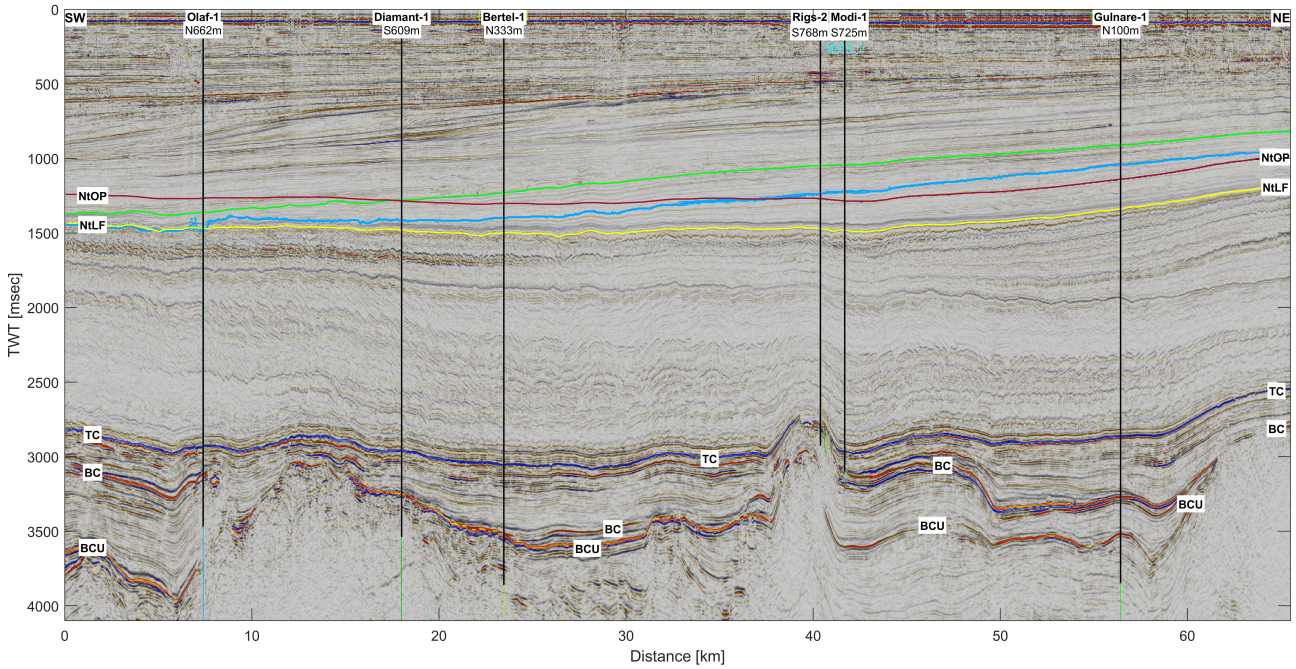

Figure 7: Regional seismic line from the Mid North Sea high (left) to the East North Sea High to the right. The dark red horizon (NtOP) approximates near top overpressure as indicated from Eaton analysis but crosses reflectors exemplified with the blue and lime-green unnamed horizons. Other horizons are: NtLF: near top Lark Formation (mid-Serravalian), TC: top Chalk, BC: base Chalk, BCU: base Cretaceous unconformity. Numbers below well names are distances in meters North (N) or South (S) of the seismic line.

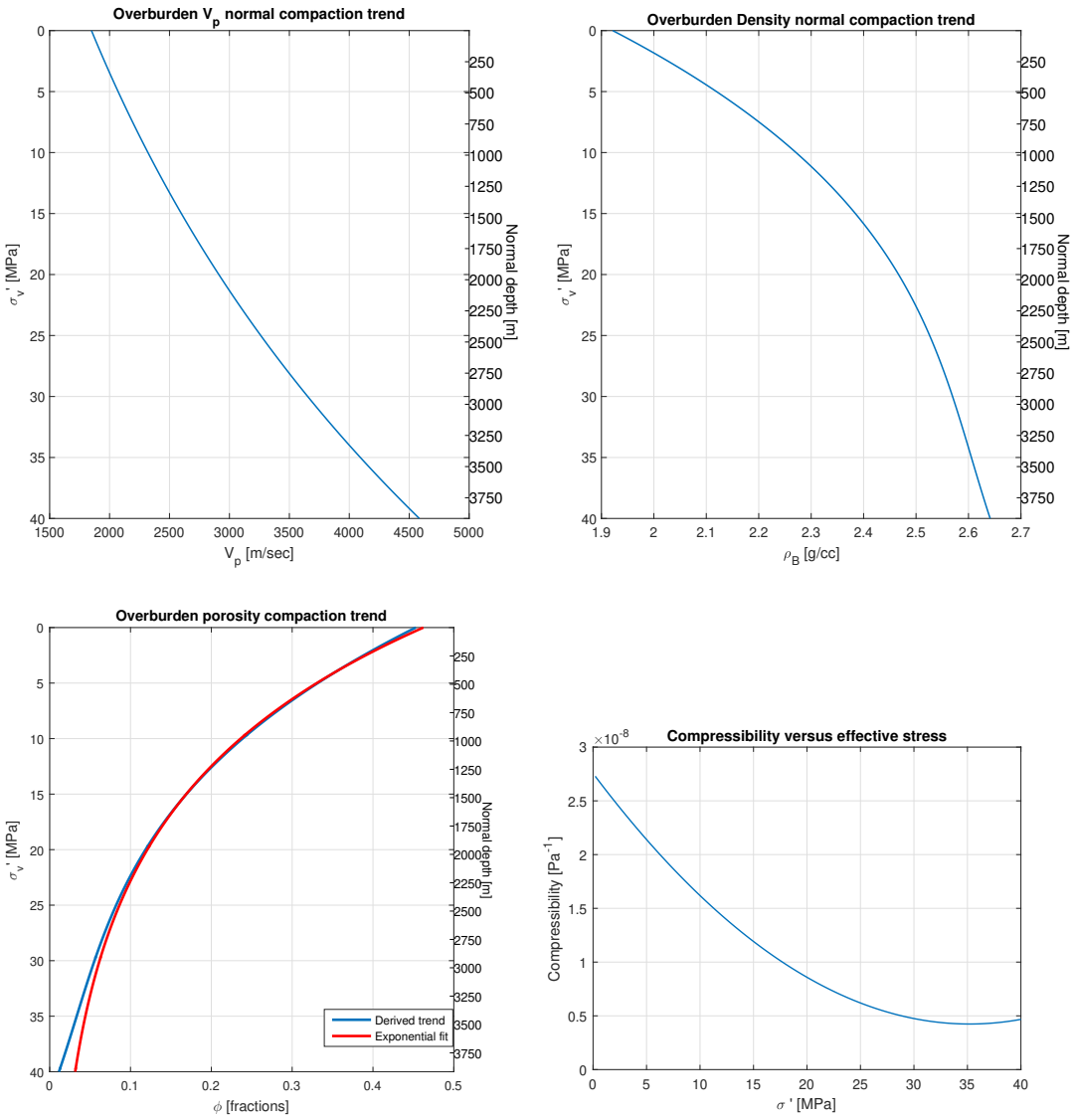

Figure 8: Upper left shows the assumed $V_p - \sigma'_v$ trend found in the Eaton analysis. To the right, density is converted to ρ_B using $\rho_B - V_p$ correlations from wells in the area. Lower left plot shows the porosity trend converted from the density trend. The derivative thereof estimates plastic compressibility as function of effective stress (lower right). The depth axes are approximations assuming hydrostatic conditions.

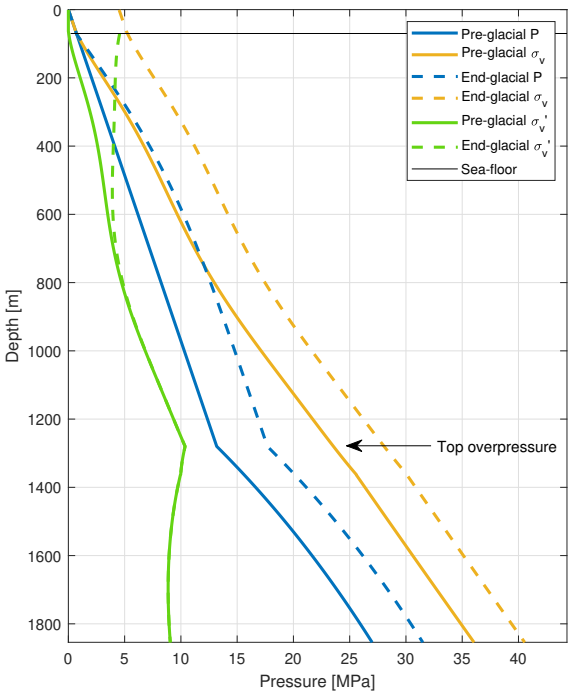

Figure 9: Experiment to show possible effects of loading by 500m of ice for 20,000 years using a pressure diffusivity 50 times larger than what was applied in the modeling of Paleogene over-pressure. Dashed lines show pressure and stress at the end of the period just before the ice melts. As the ice vanishes pressure and stress return to pre-glacial levels. The result of the effective stress increase in the upper $\sim 500m$ is that proxies for degree of compaction like interval velocity will display no or even negative depth trends in this interval (compare Fig. 4).

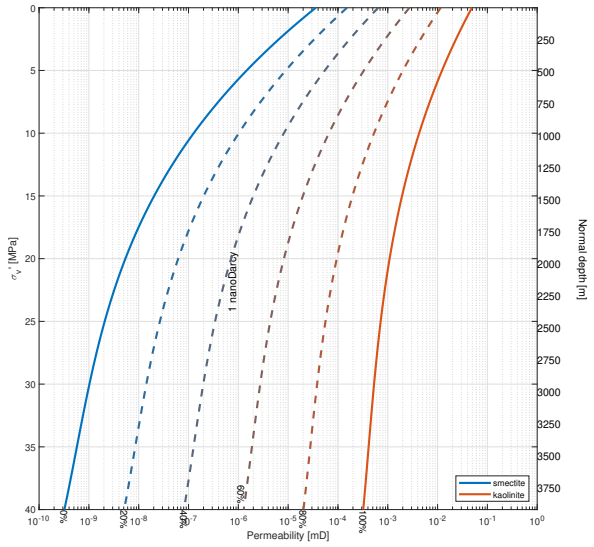

Figure 10: Calculated permeability using generic trends for mixtures of smectite and kaolinite using relationships from Mondol et al. (2008). Variation with depth is reduced compared to Mondol et al. (2008) due less variable porosity found in the area (cf. Fig. 8).

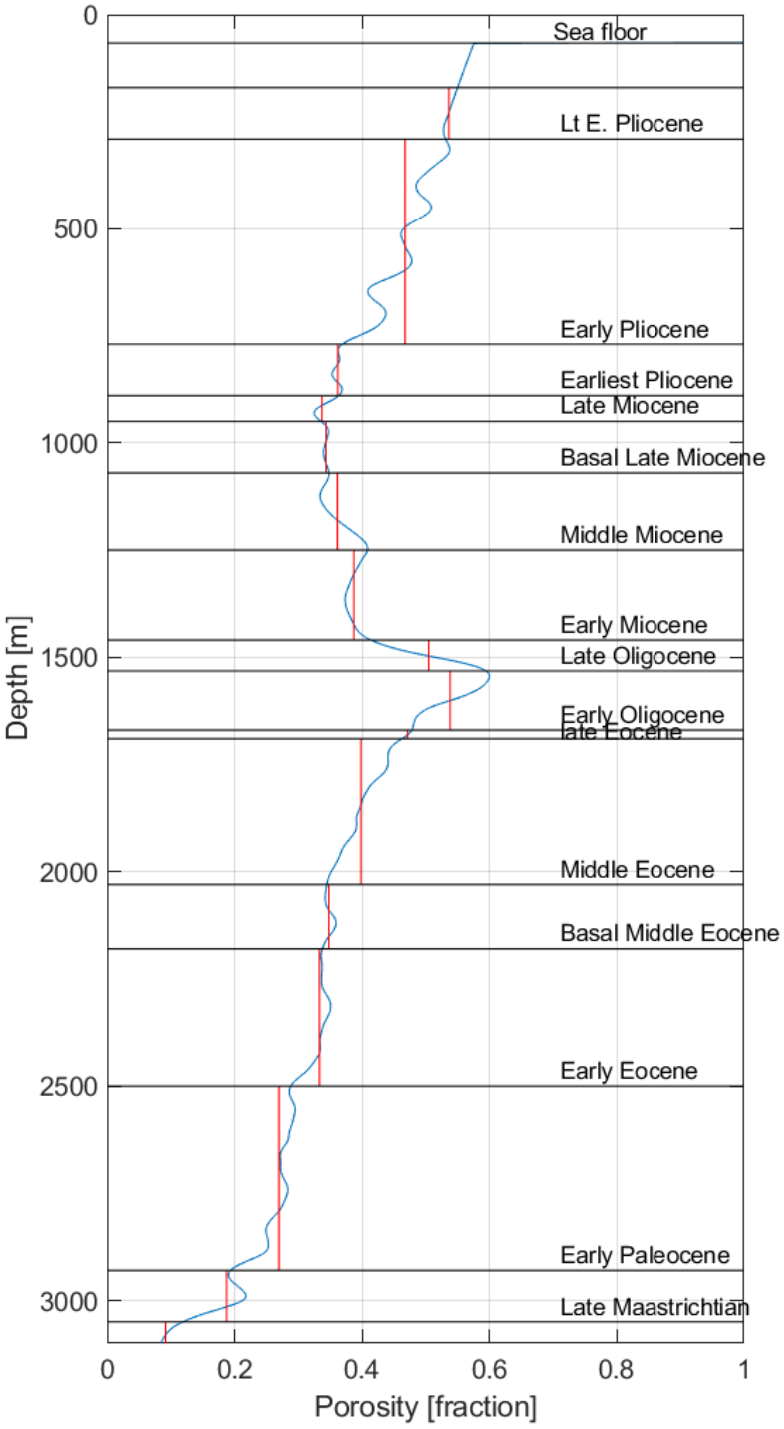

Figure 11: Porosity log for Bertel-1. The log is blocked according to stratigraphic resolution and each layer assigned compaction parameters (ϕ_0 and a, equation 7) adjusted such that forward modeling matches this log. This involves adjustment of the parameters for each layer through a few iterations.

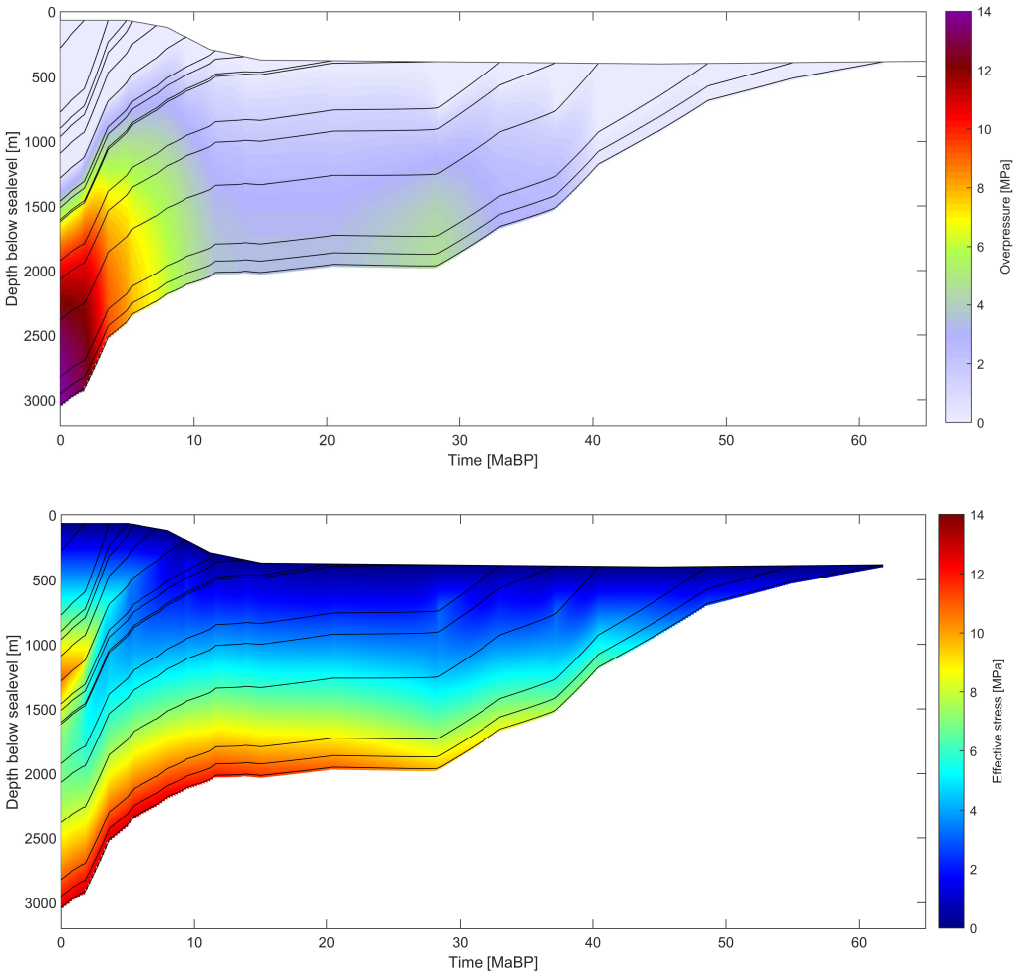

Figure 12: Overpressure development at Bertel-1 well location through time as a consequence of burial (above). Lines represent dated horizons. Below is the the calculated vertical effective stress through time. Note mid-Tertiary local maximum effective stress at present. Palaeo water depths are adapted from Gemmer et al. (2002).

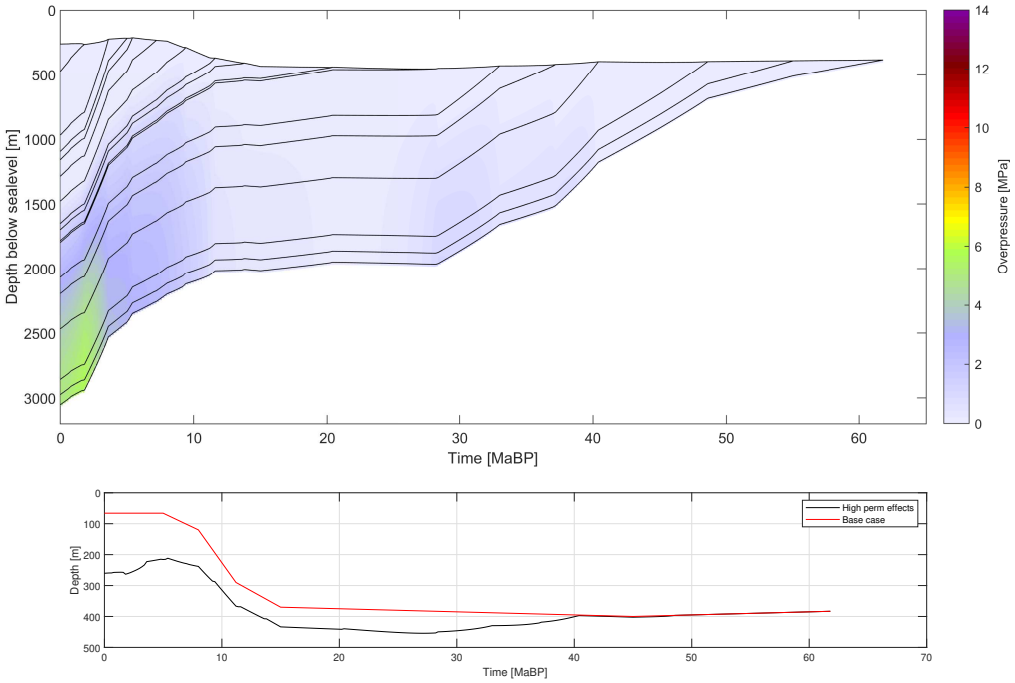

Figure 13: Overpressure development at the Bertel-1 location assuming permeability to be 10 times higher (above). The maximum overpressure barely reach $4MPa$, and compaction exceeds observations in the well. The amount of solids deposited is the same. Thus, basement loading is the same and present water depth would increase from the observed $66m$ to $260m$ (below).

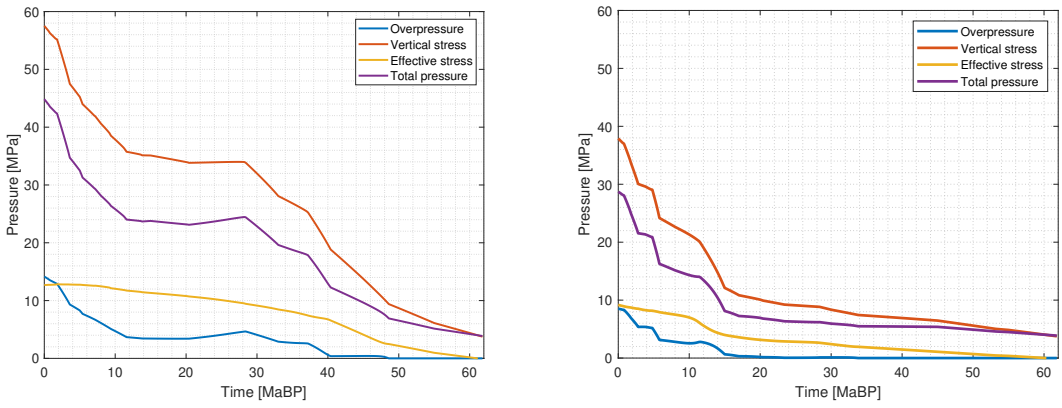

Figure 14: Calculated stresses and pressure at top chalk level through time. Left shows the Bertel-1 well (compare Fig. 7) and right shows the Nana-1 well. The effective stress is seen to increase through time only as required for the Eaton method to work.

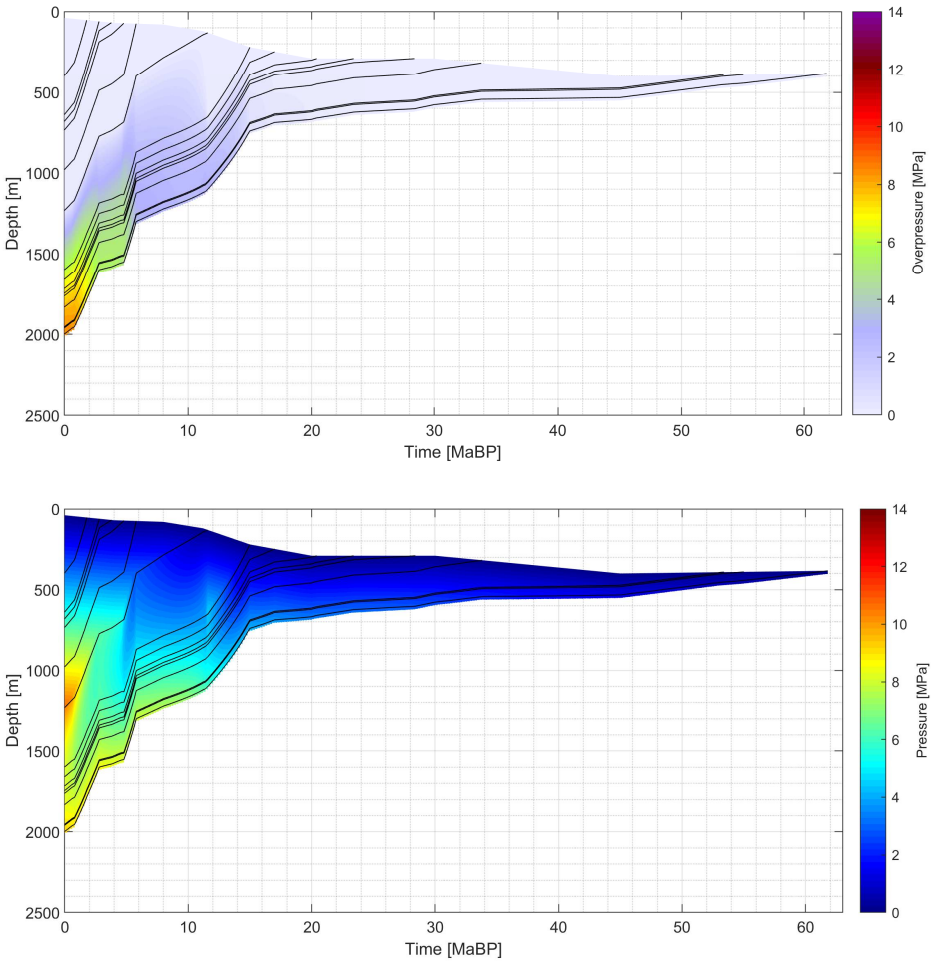

Figure 15: Overpressure development calculated for the Nana-1 well through time as a consequence of burial (above). Colorscales match those in Fig. 12. Lines represent dated horizons. Below is the the calculated vertical effective stress through time. Palaeo water depths are adapted from Gemmer et al. (2002).

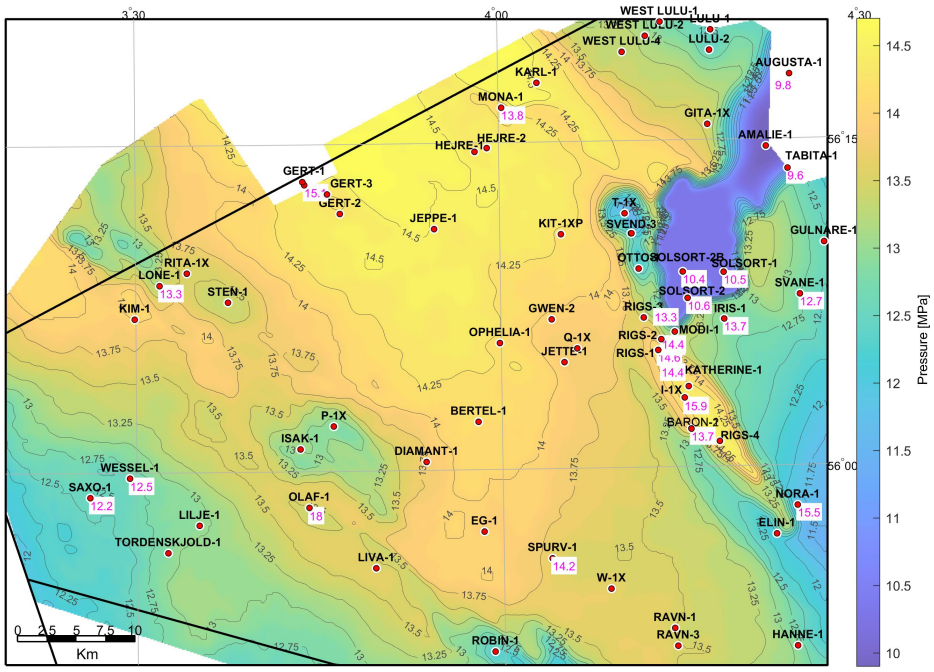

Figure 16: Map of overpressure for the upper Chalk (values in MPa). Small white boxes are measured pressures from wells. An anomalously low overpressure is due to Paleocene sands that partially drain overpressure. Observations exceeding the mapped estimate are deemed indicative of (partial) connection to high Jurassic pressures. Location in Fig. 1.

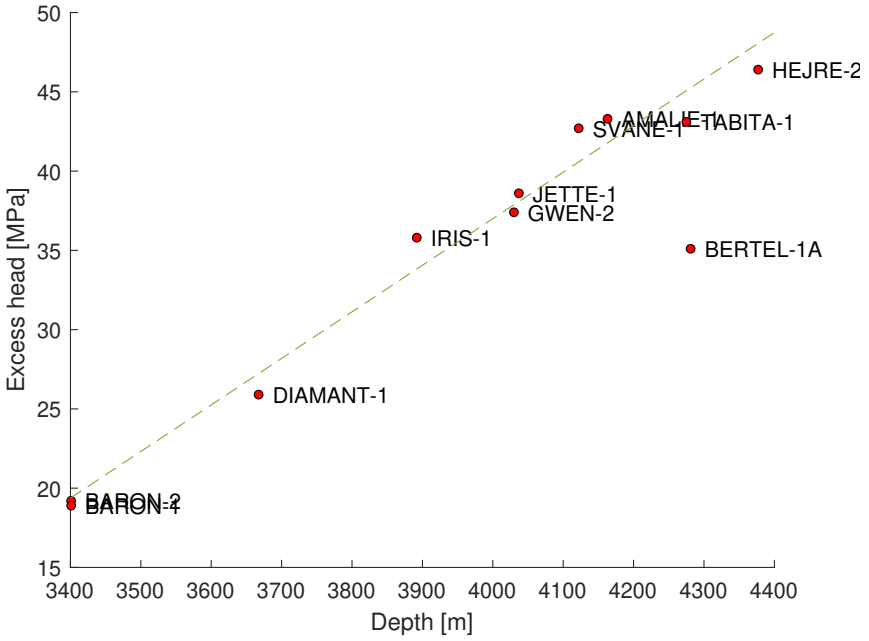

Figure 17: Cross-plot of top Jurassic depth versus degree of overpressure as recorded by RFT, MDT data. The good correlation is likely due to the control by the maturity level of the main Jurassic source rock which in turn correlates with depth. Bertel-1 is the only anomaly; likely due to poorer source rock (Petersen et al. 2010). Application of such empirical correlations for pressure prediction should however be used with caution.

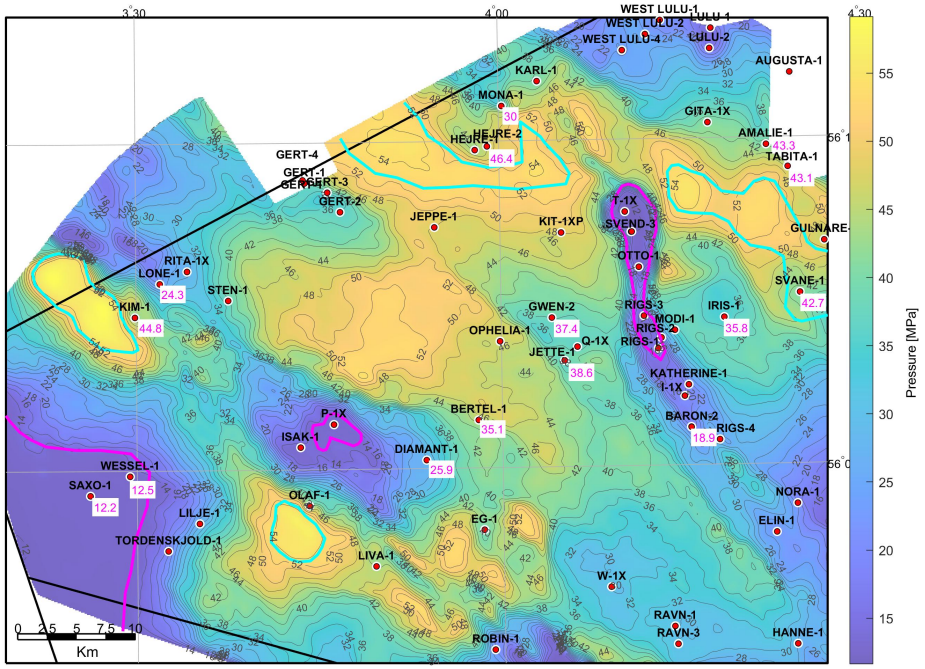

Figure 18: Map of pressure above hydrostatic for the uppermost Jurassic (values in MPa). Small white boxes are pressure measurements (above hydrostatic) from wells. Only the Bertel-1 well is poorly matched. Pink lines delineate areas where pre-Cretaceous overpressure is very similar to upper chalk overpressure, and light green lines delineate areas, where Jurassic overpressure is at or close to the fracture gradient (extreme pressure). As the map uses an empirical correlation for mapping, it should be used by great caution.